International Journal of Thermal Sciences 148 (2020) 106062

Contents lists available at ScienceDirect

International Journal of Thermal Sciences

journal homepage: www.elsevier.com/locate/ijts

Correction for semi-infinite assumption in the theories of natural convection and determination of average Nusselt number for finite inclined plates

Abhijit Guha*, Kaustav Pradhan, Akshat Jain

Mechanical Engineering Department, Indian Institute of Technology Kharagpur, Kharagpur, Pin 721302, India

ARTICLE INFO

Keywords:
Natural convection
Inclined plates
CFD
Buoyant plume
Heat transfer

ABSTRACT

It is established that large errors would be incurred if the average Nusselt number for natural convection above heated horizontal plates of finite size is determined by the similarity or integral theories which assume the plate is semi-infinite. Recognizing that boundary layers grow from both edges of a finite plate, correction factors are mathematically deduced for the isothermal case ($F_t = 2^{2/5}$) and for the case of constant heat flux ($F_q = 2^{1/3}$). Correction factors are also developed for near-horizontal orientations of the heated plate. The semi-infinite assumption does not alter the computation of the overall heat transfer rate for inclination angles at which the vertical mechanism of natural convection is dominant since then, even in the case of a finite plate, a single boundary layer covers the entire length of the plate. The theoretical rationalization developed in the paper brings the predictions of explicit algebraic expressions for average Nusselt number in line with those determined accurately by computational fluid dynamics (with extensive experimental verification), and provides physical explanation of the subtle thermo-fluid-dynamics of natural convection established by the present CFD simulations.

1. Introduction

Natural convective flow is set up in a fluid due to density gradients that are in turn developed due to temperature differences in the fluid. Heat transfer by natural convection is an important physical phenomenon and is often encountered in engineering devices such as electronic equipments, nuclear reactors, etc. Natural convection flows adjacent to plate-like geometries are of interest in a number of industrial applications such as the heat treatment of materials travelling between a feed roll and a wind-up roll or on conveyor belts, the hot extrusion of steel, the lamination and melt-spinning processes in the extrusion of polymers, etc. [1].

Calculation of the overall heat transfer rate in natural convection, and therefore of the average Nusselt number $\overline{Nu}$, for a heated finite plate is important from a practical point of view. From the value of $\overline{Nu}$ one may directly determine by how much the overall heat transfer changes as the orientation of the plate is altered from the horizontal to vertical. Recently, Guha and Pradhan [2] applied the integral method to formulate a set of simple generic equations that represents natural convection on horizontal, inclined and vertical surfaces subjected to arbitrary variation in wall temperature or surface heat flux for a wide range of parameters ($10^3 \leq Gr \leq 10^7$, $0.01 \leq \mathrm{Pr} \leq 100$ and $0° \leq \gamma \leq 90°$). They quantified, for the first time, the relative contribution of the horizontal and vertical mechanisms of natural convection on an inclined surface. In two recent papers the power of computational fluid dynamics (CFD) is invoked to obtain accurate solutions of natural convective flow above a heated finite horizontal plate [3] and that around a heated finite vertical plate [4]. In the present paper the same CFD method is applied to finite inclined plates with constant temperature (isothermal) or constant heat flux condition, with an extensive experimental validation of the computed heat transfer results. The subscripts t and q are used here to denote the isothermal and iso-heat-flux conditions respectively. The subscripts h and v are used here to denote the horizontal and vertical orientations respectively.

Similarity analysis of natural convection past a semi-infinite isothermally heated vertical plate is now a standard element of all books on convection [5–8]. Laminar natural convection on a vertical plate has been studied by experiments [9–12], similarity theory [13] and integral theory [14]. Recently, Guha and Nayek [4] performed a detailed computational study of the thermo-fluid-dynamics of natural convection past a finite vertical plate. The mechanism of natural convection above a horizontal plate is quite different from that around a vertical plate, and was termed as 'indirect natural convection' by Schlichting and Gersten [8] due to the nature of its generation. Natural convection over a heated horizontal surface has been studied using similarity theory [15], integral theory [16] and experiments [17]. Guha and Sengupta [3] presented a comprehensive CFD analysis of the effects of the finiteness of a heated horizontal plate on the thermo-fluid-dynamics

* Corresponding author.
E-mail address: a.guha@mech.iitkgp.ac.in (A. Guha).

https://doi.org/10.1016/j.ijthermalsci.2019.106062
Received 16 January 2019; Received in revised form 14 June 2019; Accepted 22 August 2019

Nomenclature

c_p	specific heat capacity (J/kgK)
Gr_L	Grashof number defined as $\rho_\infty^2 g\beta(T_w - T_\infty)L^3/\mu^2$ for isothermal case
Gr_L^*	Grashof number defined as $\rho_\infty^2 g\beta q_w L^4/k\mu^2$ for constant surface heat flux case local Grashof number defined as $\rho_\infty^2 g\beta(T_w - T_\infty)x^3/\mu^2$ for isothermal case
Gr_x^*	local Grashof number defined as $\rho_\infty^2 g\beta q_w x^4/k\mu^2$ for constant surface heat flux case
g	acceleration due to gravity (m/s^2)
h_x	local convective heat transfer coefficient (W/m^{2}K)
$\overline{h}$	average convective heat transfer coefficient (W/m^{2}K)
k	thermal conductivity (W/mK)
L	length of plate (m)
Nu_x	local Nusselt number defined as $h_x x/k$
$\overline{Nu}$	average Nusselt number defined as $\overline{h}L/k$
Pr	Prandtl number defined as $\mu c_p/k$
p	static pressure (Pa)
p_∞	ambient pressure (Pa)
Q	total surface heat flux (W)
q_x	local heat flux (W/m^2)
q_w	wall heat flux (W/m^2)
Ra_L	Rayleigh number defined as Gr_LPr for isothermal case
Ra_L^*	Rayleigh number defined as Gr_L^*Pr for constant surface heat flux case
Ra_x	local Rayleigh number defined as Gr_xPr for isothermal case
Ra_x^*	local Rayleigh number defined as Gr_x^*Pr for constant surface heat flux case
T	fluid temperature (K)
T_w	temperature of the heated surface (K)
T_∞	ambient temperature (K)
t_P	thickness of plate (m)
u	component of velocity along the plate (m/s)
V_Y	component of velocity along Y-direction (m/s)
v	component of velocity normal to the plate (m/s)
$\vec{v}$	velocity vector
X	horizontal co-ordinate with origin at left (or trailing) edge of the heated side of the plate
x	co-ordinate along the plate with origin at right (or leading) edge of the heated side of the plate
$\overline{x}$	non-dimensional x coordinate defined as x/L
$\overline{x}_{lift-off}$	non-dimensional lift-off distance
$\overline{x}_{q_{x,\min}}$	non-dimensional minimum wall heat flux point
Y	vertical co-ordinate with origin at left (or trailing) edge of the heated side of the plate
y	co-ordinate normal to the plate with origin at right (or leading) edge of the heated side of the plate
$\overline{y}$	non-dimensional y coordinate defined as y/L

Greek symbols

α	thermal diffusivity (m^2/s)
β	coefficient of thermal expansion ()
γ	inclination angle (degree)
μ	dynamic viscosity (Pa − s)
ρ	density (kg/m^3)
ρ_∞	density at temperature T_∞ (kg/m^3)

of natural convection above it. Apart from these, several other studies pertaining to natural convection of different types of fluids (non-Newtonian fluid, nanofluid, etc.) above horizontal surfaces may be found in Refs. [18–21]. A numerical study [22] presents detailed non-linear interaction of natural convection with von Kármán's flow on a heated rotating disc.

While it has been possible to develop self-similarity theory for vertical plate ($\gamma = 90°$) and horizontal plate ($\gamma = 0°$), the flow solutions for all other inclination angles are found to be non-similar. Similarity theories show that the Nusselt number varies as the one-fourth power of Grashof number for natural convection on an isothermal vertical surface ($Nu_x \propto Gr_x^{1/4}$) while it varies as the one-fifth power of Grashof number ($Nu_x \propto Gr_x^{1/5}$) for isothermal horizontal surfaces. Since the natural convection mechanisms for both vertical and horizontal configurations are operative in case of inclined surfaces, the development of a closed-form solution for the Nusselt number, which will reduce to the known solutions in the two limits of horizontal and vertical surfaces, is difficult. Natural convective flow adjacent to inclined plates has been investigated experimentally [23–25] as well as numerically [26–29]. While the experimental studies tried to relate the heat transfer results on inclined surfaces to the limiting cases of vertical and horizontal surfaces, the numerical studies involved the derivation and subsequent solution of non-similar boundary layer equations for natural convection on an inclined surface. Recently, a comprehensive computational study is performed for natural convection adjacent to isothermally heated finite inclined plates [30]. The detailed thermo-fluid-dynamics of the convective flow near the heated plate as well as that in the buoyant plume is discussed in Ref. [30]. The paper develops several new concepts (such as the lift-off point) and provides a thorough description of the subtle transition in the physical processes as the mechanism of natural convection changes from being induced-pressure-difference-driven to direct-buoyancy-driven as the inclination angle is changed from zero (horizontal) to 90° (vertical).

All integral and similarity analyses of natural convection adjacent to flat plates are restricted by some assumptions: (i) the plate is semi-infinite, (ii) the boundary layer equations are valid, (iii) there is no buoyant plume (iv) the plate thickness is negligible, and (v) the flow occurs on only one side of the plate. In order to ensure self-similarity, sometimes non-physical boundary conditions may also be used [4]. In spite of the limitations, some theoretical analyses [2,16] provide algebraic expressions for Nusselt number as explicit functions of Grashof number, Prandtl number and inclination angle (see the Appendix for a short description of important explicit correlations). This has obvious practical utility. The theoretical analyses are also useful in comprehending results obtained from CFD studies or experiments. With this in mind, values of average Nusselt number ($\overline{Nu}$) for the isothermal and iso-heat-flux cases are computed by integrating the results for local Nusselt number Nu_x given in three previous theoretical work [2,27,28]. When these values of $\overline{Nu}$ are compared with those obtained from the present CFD simulations, large differences are found for the horizontal plate and near-horizontal orientations ($0° \le \gamma \le 15°$). There is a second important difference between the CFD results and predictions of theories. The present CFD results, for both isothermal and iso-heat-flux cases, show that as the inclination angle is increased gradually from the horizontal position, the value of average Nusselt number $\overline{Nu}$ initially decreases slightly, passes through a minimum point and then onward increases continuously up to the vertical position of the plate. $\overline{Nu}$ constructed by integrating theories of [2,27,28], on the other hand, show monotonic increase from the horizontal to vertical.

The present paper provides theoretical explanation for the above-mentioned discrepancy in the values of average Nusselt number $\overline{Nu}$ determined by the present CFD simulations and those given by previous theoretical analyses. It is shown that, since a practical plate is of finite length, and convective flow may be induced on both sides of the plate,

with a deviation from boundary-layer type of flow (such as formation of buoyant plume), the afore-mentioned assumptions inherent in previous theoretical analyses may lead to inability of the solution in capturing all the intricate features of the flow field. Correction factors are developed that would bring the theoretical analyses in line with CFD results. The process of mathematical deduction provides physical insight and helps in comprehending the CFD results.

2. Mathematical formulation

The present study considers steady laminar natural convective flow around a heated plate inclined at an angle γ to the horizontal (Fig. 1). The governing equations for the above-mentioned flow system are given below:

$$\frac{\partial \rho}{\partial t} + \vec{\nabla}.(\rho\vec{v}) = 0 \tag{1}$$

$$\frac{\partial(\rho\vec{v})}{\partial t} + \vec{\nabla}.(\rho\vec{v}\vec{v}) = -\vec{\nabla}p + \vec{\nabla}.\left(\mu\vec{\nabla}\vec{v} + \mu\vec{\nabla}\vec{v}^{T} - \frac{2}{3}\mu\vec{\nabla}.\vec{v}\right) + \rho\vec{g} \tag{2}$$

$$\frac{\partial(\rho T)}{\partial t} + \vec{\nabla}.(\rho\vec{v}T) = \vec{\nabla}.\left(\frac{k}{c_p}\vec{\nabla}T\right) + \Phi \tag{3}$$

In equations (1)–(3), $\vec{v}$ denotes the velocity vector, p is the static pressure and T is the temperature of the fluid. ρ, μ, c_p and k are respectively the density, dynamic viscosity, specific heat capacity at constant pressure and thermal conductivity of the fluid. $\vec{g}$ is the gravity vector. The viscous dissipation term Φ which is usually small [31] for natural convection is neglected in the present study. Density of the fluid is considered to be constant except in the body force term in equation (2). The Boussinesq approximation, which considers a linear variation of density with temperature rise, is adopted here for the variation of density in the body force term. According to the Boussinesq approximation,

$$\rho = \rho_\infty[1 - \beta(T - T_\infty)] \tag{4}$$

where β is the thermal expansion coefficient of the fluid, T_∞ and ρ_∞ are respectively the temperature and density of the quiescent fluid far away from the heated plate. All the other thermo-physical properties of the fluid like dynamic viscosity, specific heat capacity and thermal conductivity are considered to be constant.

A two-dimensional analysis is performed here for which the width of the plate perpendicular to the plane of the paper is assumed infinite. The x-coordinate is taken along the plate and the y-coordinate is measured normal to the plate (Fig. 1). The origin of the co-ordinate system is taken at point O which is the lowest point on the heated surface (right-most point for horizontal configuration). The velocity component along the x-direction (along the plate) is u. The velocity component along the y-direction (normal to the plate, pointing away from the plate on the heated side of the plate) is v. It is to be noted that, with respect to any globally fixed co-ordinate system, the co-ordinate axes x and y (and hence u and v) rotate with the plate as its inclination is varied. Gravity $\vec{g}$ acts vertically downwards, which is in the negative y-direction for the horizontal plate orientation ($\gamma = 0°$).

The heat transfer results in the study of natural convection adjacent to a flat plate are usually presented in terms of the Nusselt number (Nu) or the convective heat transfer coefficient (h). The local heat flux at any position (x) along the plate is computed using the following expression:

$$q_x = -k\left(\frac{\partial T}{\partial y}\right)_{y=0} \tag{5}$$

where x and y are respectively the coordinates along and normal to the plate.

The local convection heat transfer coefficient h_x is given by:

$$h_x = \frac{q_x}{(T_w - T_\infty)} \tag{6}$$

The local Nusselt number (Nu_x) is evaluated from the local convective heat transfer coefficient (h_x) according to the following expression:

$$Nu_x = \frac{h_x x}{k} \tag{7}$$

where x is the distance along the plate from the leading (right) edge and k is the thermal conductivity of the fluid. The average Nusselt number ($\overline{Nu}$) is evaluated from the following expression:

$$\overline{Nu} = \frac{\bar{h}L}{k} \tag{8}$$

where L is the length of the plate and $\bar{h}$ is the average convective heat transfer coefficient that is calculated from h_x using the following expression:

$$\bar{h} = \frac{1}{L}\int_0^L h_x dx \tag{9}$$

3. Computational fluid dynamic simulations

The governing equations for natural convective flow (equations (1)–(3)) around an inclined plate are solved using a commercial finite-volume based CFD solver Fluent [32]. Two-dimensional simulations are performed with the assumption that the dimension of the plate in the direction perpendicular to the plane shown in Fig. 1 is infinitely large. A structured mesh is constructed for the chosen computational domain using ANSYS Meshing and a systematic grid independence study is performed.

3.1. Geometry, grid and boundary conditions

A flat plate of length L and thickness t_P (= $L/100$) is considered in the present study. It is assumed that one side of the plate is maintained at a temperature T_w ($>T_\infty$) or subjected to a uniform heat flux q_w while the other three sides are insulated (i.e. adiabatic condition is maintained there). In their experiments, Rich [23], Vliet [24] and Sang-Urai [25] used an insulated surface ($q_w = 0$) for the side of the inclined plate opposite to the heated side. We have also used the adiabatic ($q_w = 0$) boundary condition for that side of the plate. However, there is no explicit mention of the condition on the two edges along the thickness (t_P) of the plate used in the experiments. We have used the adiabatic condition there so that it does not affect the total heat transfer from the plate (and hence the Nusselt number calculations). The no-slip and no-penetration boundary conditions are applied on all the four sides of the plate. Mathematically, the boundary conditions for the four sides of the plate may be listed as follows:

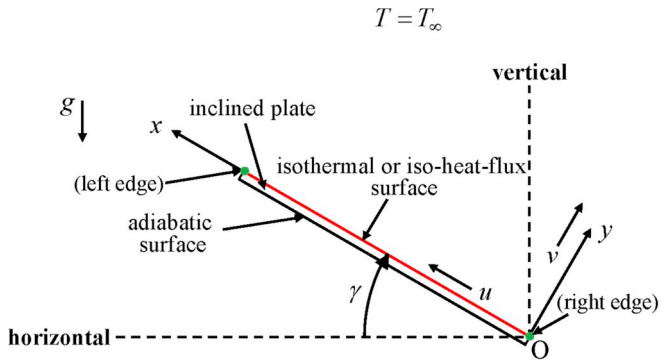

Fig. 1. A physical model and coordinate system for the analysis of natural convection around a heated inclined plate.

Heated side of plate:

$$\text{At } y = 0,\ 0 \le x \le L:\ u = v = 0,$$
$$:T = T_w \text{ (isothermal) or } -k\frac{\partial T}{\partial y} = q_w \text{ (iso-heat-flux)} \tag{10}$$

Other three sides of plate:

$$\text{At } x = 0,\ -t_P \le y \le 0:\ u = v = 0,\ \frac{\partial T}{\partial y} = 0. \tag{11}$$

$$\text{At } x = L,\ -t_P \le y \le 0:\ u = v = 0,\ \frac{\partial T}{\partial y} = 0. \tag{12}$$

$$\text{At } y = -t_P,\ 0 \le x \le L:\ u = v = 0,\ \frac{\partial T}{\partial y} = 0. \tag{13}$$

Fig. 2 shows the computational domain for the case $\gamma = 90°$ (vertical). The "pressure outlet" boundary condition available in Fluent is applied at the periphery of the overall computational domain. In Fluent, when the gravitational acceleration is activated in the simulation of incompressible flow, the static pressure p at a point is re-defined as $p' = p - \rho_\infty \vec{g}\cdot\vec{r}$ [32], where ρ_∞ is the ambient density of the fluid (which is assumed constant), $\vec{g}$ is the gravitational acceleration and $\vec{r}$ is the position vector. The "pressure outlet" boundary condition feature requires the specification of the re-defined (gauge) static pressure p'. Since the hydrostatic pressure is already contained in the modified pressure p', setting $p' = 0$ on all the boundaries of the overall computational domain automatically sets $p = p_\infty$ there, p_∞ being the ambient pressure that varies in the direction of gravity according to the hydrostatic equation.

In the present study, we have considered laminar flow. The fluid flow over an inclined plate due to natural convection becomes unstable above a critical value of Ra_L. In case of vertical flat plate the critical value of Ra_L is 9×10^9 [33,34], while the transition from laminar to turbulent flow takes place at about $Gr\mathrm{Pr} = 8 \times 10^6$ for a horizontal plate [35]. The present theoretical study with parametric variation in the inclination angle γ is conducted at $Gr_L = 10^6$ (or $Gr_L^* = 10^6$) and $\mathrm{Pr} = 0.7$ so that the flow remains laminar above the plate. This also ensures that the flow in the buoyant plume remains laminar [36]. Later, for experimental verification, several additional CFD simulations are run at various values of Rayleigh number to match corresponding experimental conditions available in the literature (Sections 4.1 and 4.2).

3.2. Numerical schemes

The governing equations (1)–(3) are solved numerically using the pressure-based solver available in FLUENT. All transport equations are discretized to be second order accurate in space. The second order upwind scheme provided in Fluent is used for the discretization of the advection terms, while the central difference scheme is used for discretizing the diffusion terms in the momentum and energy equations. The SIMPLE algorithm is used for pressure-velocity coupling. Under-relaxation factors are suitably employed such that numerical instabilities are avoided but computational time does not increase excessively. A segregated implicit [37] solver is used to solve the resulting system of discretized equations. The solver uses a time-marching technique [38,39] to obtain a steady-state solution as the limiting process of an unsteady simulation. In all simulations, a solution is said to be converged if the scaled residuals reach 10^{-6} for all the governing equations (which is considerably smaller than what is normally set in much of the reported CFD work). A large number of grid points and double precision arithmetic are used to obtain high precision of the computed results.

3.3. Domain independence test

We have performed separate domain independence tests for the various inclination angles considered in the present work. However, here we present only the results for the isothermal case at $\gamma = 45°$ for brevity, as an illustrative example of the adopted procedure. In order to perform a systematic domain independence test, we have used the same grid structure for all the domains.

Table 1 shows that as the size of the computational domain (in terms of l_x and l_y) is systematically increased, the values of the computed average Nusselt number $\overline{Nu}$ uniformly converge. Between domains D2 and D3, there is no difference in $\overline{Nu}$ up to the second decimal place and the relative change in the value is less than 0.01%. Accordingly, domain D2 is considered adequate for $\gamma = 45°$ and is used for all subsequent simulations at $\gamma = 45°$.

Following a similar procedure, separate domain independence tests are carried out at each angle of inclination, which specify the particular values of l_x and l_y that are appropriate for the particular angle of inclination. The size of the computational domain therefore varies according to the orientation of the plate.

3.4. Grid independence test

A systematic grid independence study is reported below for an inclination angle of 45° and Pr = 0.7. Three grid structures are constructed—viz., "coarse", "medium" and "fine" — as shown in Table 2. The value of Δy_1 is progressively decreased as the grid is progressively refined from "coarse" to "fine." A non-uniform grid distribution (with $\Delta x_1 = \Delta y_1$ and geometric progression ratio of 1.02) is used in both x and y– directions so that the natural convective boundary layer is appropriately resolved, and at the same time, a large computational domain can be utilized so that the boundary conditions for the natural

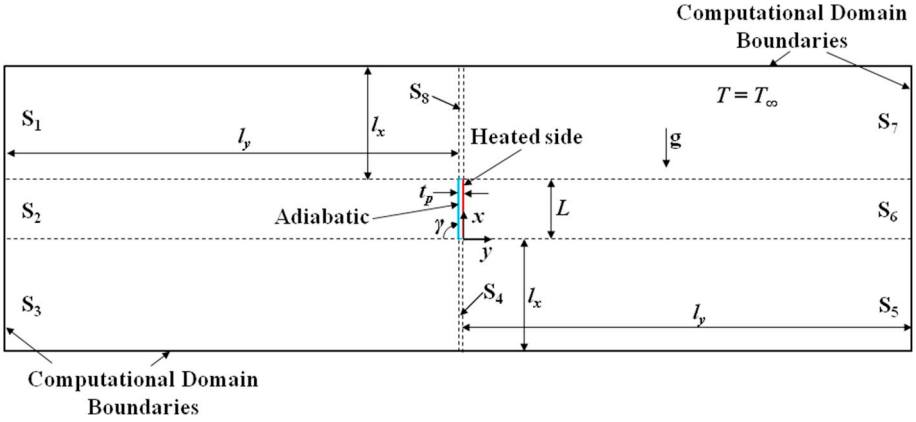

Fig. 2. The schematic details of the computational domain for $\gamma = 90°$ used in the present CFD analysis.

Table 1
Results of the domain independence test for three computational domains at $\gamma = 45^\circ$ ($Gr_L = 10^6$, Pr = 0.7).

Name of the computational domain	l_x/L	l_y/L	$\overline{Nu}_t$
D1	2	2	14.7999
D2	4	4	14.8284
D3	8	8	14.8299

Table 2
Results of the grid independence test for three grid distributions in domain D2 ($\gamma = 45^\circ$, Pr = 0.7, $Gr_L = 10^6$ for isothermal or $Gr_L^* = 10^6$ for iso-heat-flux case).

Grid distribution	First grid size adjacent to plate, Δy_1 (m)	Number of computational elements	$\overline{Nu}_t$(isothermal)	$\overline{Nu}_q$(iso-heat-flux)
Coarse	0.0001	394272	14.7911	9.9670
Medium	0.000075	489804	14.8243	9.9779
Fine	0.00005	799784	14.8284	9.9834

convective flow can be applied appropriately. The size of the grid is allowed to grow only up to set limits. Corresponding to the fine grid, there are 1020 grid points on the heated surface of the plate. Similarly, the flow fields around the plate corners are finely resolved as the minimum size of a computational element there is $\Delta y_1 \times \Delta y_1$.

Table 2 shows that as the grid size is systematically refined (following the method described above) from "coarse" to "fine", the values of the computed average Nusselt number $\overline{Nu}$ uniformly converge. Between the "medium" and "fine" grid structures for $Gr_L = 10^6$ or $Gr_L^* = 10^6$ (at which the parametric study for inclination angle is conducted in the present paper), the relative change in the value of $\overline{Nu}$ is less than (or of the order) 0.05%. Although the "medium" grid would have been considered adequate on the basis of the grid independence data alone (Table 2), the "fine" grid with 799,784 computational elements is used for all subsequent simulations for $\gamma = 45^\circ$ for improved precision of computed results and quality of the flow visualization diagrams.

4. Results and discussion

CFD simulations are run for various combinations of the Grashof number and Prandtl number at various values of the inclination angle in the range $0^\circ \le \gamma \le 90^\circ$ for a thorough understanding of the thermo-fluid-dynamics of natural convection on a heated (isothermal or constant heat-flux condition) inclined plate. Comparisons are made with existing experimental and theoretical results. For streamlining the discussion, the results are divided into a few subsections.

4.1. Natural convection around heated inclined plates for isothermal condition

The present study with parametric variation in the inclination angle γ is conducted at $Gr_L = 10^6$ and Pr = 0.7 so that the flow remains laminar above the plate. The following constant values of the parameters are used to obtain the above-mentioned values of the non-dimensional parameters: $T_w = 325$ K, $T_\infty = 300$ K, $\rho_\infty = 1.1614$ kg/m^3, $\beta = 0.00333$ K^{-1}, $\mu = 3.32 \times 10^{-5}$ Pa − s, $k = 0.04773$ W/(mK), $c_p = 1007$ J/(kgK) and $L = 0.1$ m. It was shown in Guha and Pradhan [2] that for Pr~1, the natural convection mechanism for a vertical surface is the dominating factor for a large range of inclination angles except for near-horizontal configurations. Accordingly, here we have chosen the three inclination angles at which the velocity and temperature contours are presented; $\gamma = 0^\circ$ (horizontal), $\gamma = 5^\circ$ (where horizontal mechanism dominates) and $\gamma = 90^\circ$ (vertical).

The contours of velocity for three inclination angles are shown in Fig. 3. For the horizontal ($\gamma = 0^\circ$) and near-horizontal ($\gamma = 5^\circ$) orientations, two boundary layers develop from the two edges of the plate on its heated side. For the vertical ($\gamma = 90^\circ$) orientation, a single boundary layer starting from the bottom edge of the plate (on its heated side) covers its entire length. The convective velocities in the boundary layer near the plate for the vertical orientation are significantly greater than those for the horizontal and near-horizontal orientations. The finiteness of the size of the plate results in the formation of a buoyant plume that occurs at the trailing (top) edge for $\gamma = 90^\circ$ and above the centre of the plate for $\gamma = 0^\circ$. For $\gamma = 5^\circ$, the buoyant plume rises from the plate at a location (defined as the lift-off point [30], the procedure of its determination being fully described also in Ref. [30]) in between the left edge and the centre of the plate. The distance of the lift-off point from the left edge is referred to as L_{LE} while that from the right edge of the plate is defined as L_{RE}. It is noted that the location of the lift-off point is sensitive to inclination angle γ. For an inclination angle as small as 5°, the thermo-fluid-dynamics changes significantly from what exists in the horizontal position, and the lift-off point shifts by a large distance towards the trailing edge of the plate. Fig. 3 shows that as the vertical

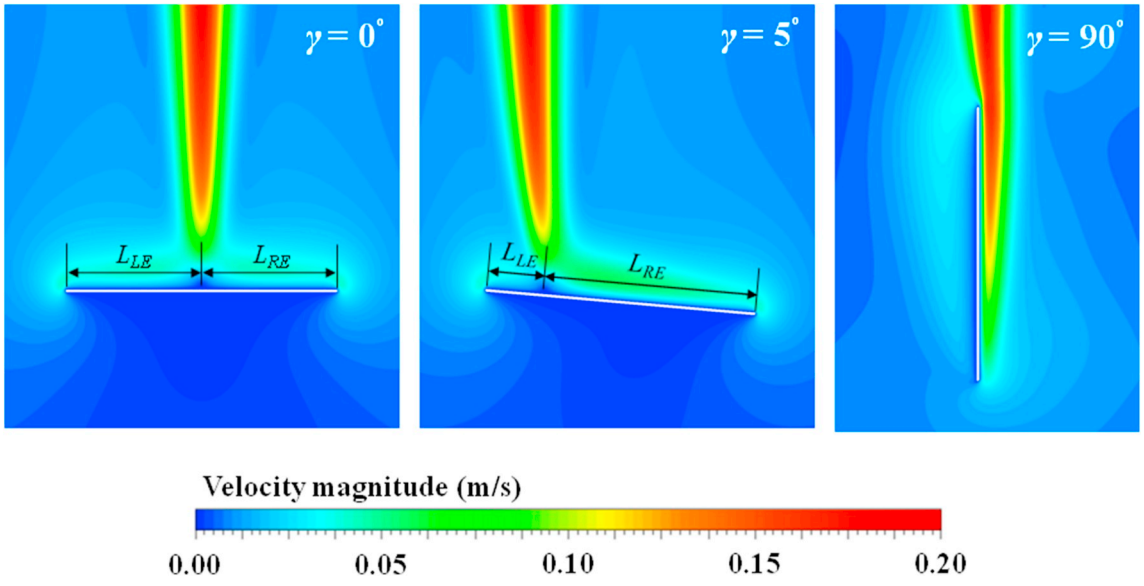

Fig. 3. Contours of velocity magnitude at three inclinations for isothermal case: prediction of present CFD simulations (Pr = 0.7, $Gr_L = 10^6$, $T_w - T_\infty = 25$ K).

distance above the plate increases, the plume-width and the maximum velocity in the plume increases due to entrainment of fluid from both sides. A small movement of the fluid can be observed on the insulated side of the vertical plate as well. For the horizontal and near-horizontal orientations, a stagnation region starts developing on the insulated side of the plate.

Fig. 4 shows the temperature contours for the same three inclination angles. Unlike the contours of velocity, the temperature is found to reach the ambient value relatively close to the heated plate (in all regions except in the buoyant plume) for all inclination angles shown. While it is found from the velocity contours (Fig. 3) that the maximum velocity in the plume increases as the vertical distance from the plate increases, Fig. 4 shows that the maximum value of the temperature inside the buoyant plume decreases as the vertical distance above the plate increases.

Fig. 5 shows the variation of the non-dimensional wall heat flux on the isothermally heated side of the inclined plate for four inclination angles in the range $0° \le \gamma \le 90°$. Each curve passes through a minimum point ($q_{x,\min}$) whose location ($\bar{x}_{q_{x,\min}}$) shifts from the centre of the plate for the horizontal position ($\gamma = 0°$) to near the trailing edge for the vertical position ($\gamma = 90°$). The principal reason for the existence of the minimum heat flux point may change depending on the inclination angle. For the horizontal and near-horizontal positions, where the buoyant plume forms within the heated side of the plate, reduced heat transfer underneath the plume (due to uplifting of the fluid as a result of confluence of two oppositely moving streams) is responsible. However, for such orientations of the plate where the vertical mechanism of natural convection is dominant [2], the surface heat flux steadily decreases toward the trailing edge due to the continuous thickening of the boundary layer (the temperature difference $T_w - T_\infty$ remaining constant) until a point is reached close to the trailing edge where edge-effects increase the wall heat flux. The minima shown for $\gamma = 0°$ and $\gamma = 5°$ occur due to the first effect, while the minima shown for $\gamma = 45°$ and $\gamma = 90°$ exist due to the second effect.

It is observed that the value of $q_{x,\min}$ increases as the orientation of the plate is changed from the horizontal to the vertical. However, the rate of increase of $q_{x,\min}$ as well as the rate of shift of $\bar{x}_{q_{x,\min}}$ decreases with increasing values of γ. For near-horizontal inclinations, where the buoyant plume lifts off from the heated surface before the trailing (left) edge of the plate is reached, $\bar{x}_{q_{x,\min}}$ approximately coincides with $\bar{x}_{lift-off}$ (location of lift-off point on the heated surface of the plate). However, unlike $\bar{x}_{lift-off}$, the minimum heat flux point never quite reaches the trailing edge of the plate because of the finiteness of the real plate

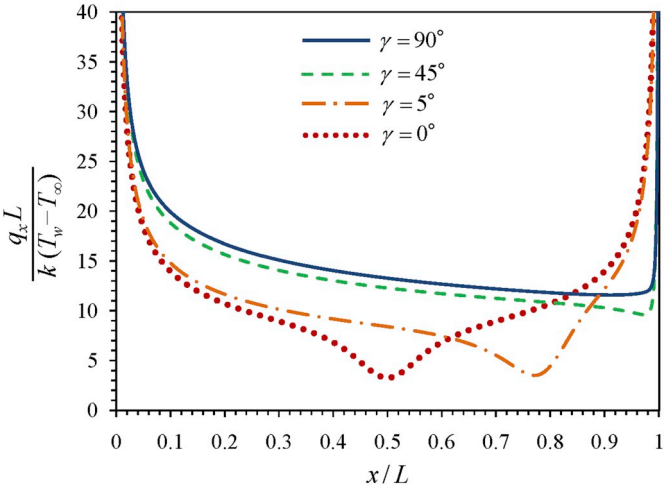

Fig. 5. Variation of non-dimensional local wall heat flux along the plate at various angles of inclination in the range $0° \le \gamma \le 90°$ (at $Gr_L = 10^6$, Pr = 0.7).

which results in high heat transfer rate at the trailing edge of the plate.

The average Nusselt number for an isothermally heated plate can be determined from the following formulation:

$$\overline{Nu}_t = \frac{\bar{h}L}{k} = \frac{L}{k}\frac{1}{L}\int_0^L h_x dx = \frac{1}{k(T_w - T_\infty)}\int_0^L q_w dx. \tag{14}$$

For accurate determination of the Nusselt number, a large number of grid points, approximately 0.7–0.9 million points depending on the inclination angle, is used in the present CFD simulations. Table 3 shows that both local and average Nusselt numbers determined by the present CFD simulations agree well with experimental values.

4.1.1. Correction factor for isothermal horizontal plate

Table 4 shows the present CFD results for $\overline{Nu}_t$ vis-à-vis the values of $\overline{Nu}_t$ that can be computed by integrating the results for Nu_x given in two previous theoretical work [2,27]. Yu and Lin [27] had numerically solved, by finite-difference method, the boundary layer equations for natural convection around a semi-infinite heated inclined plate, using a complex co-ordinate transformation. Guha and Pradhan [2] formulated a unified integral theory for arbitrary inclination, in which the orders of polynomial representing the velocity and temperature profiles could be optimized. Table 4 shows that in the range of angles $15° \le \gamma \le 90°$ the

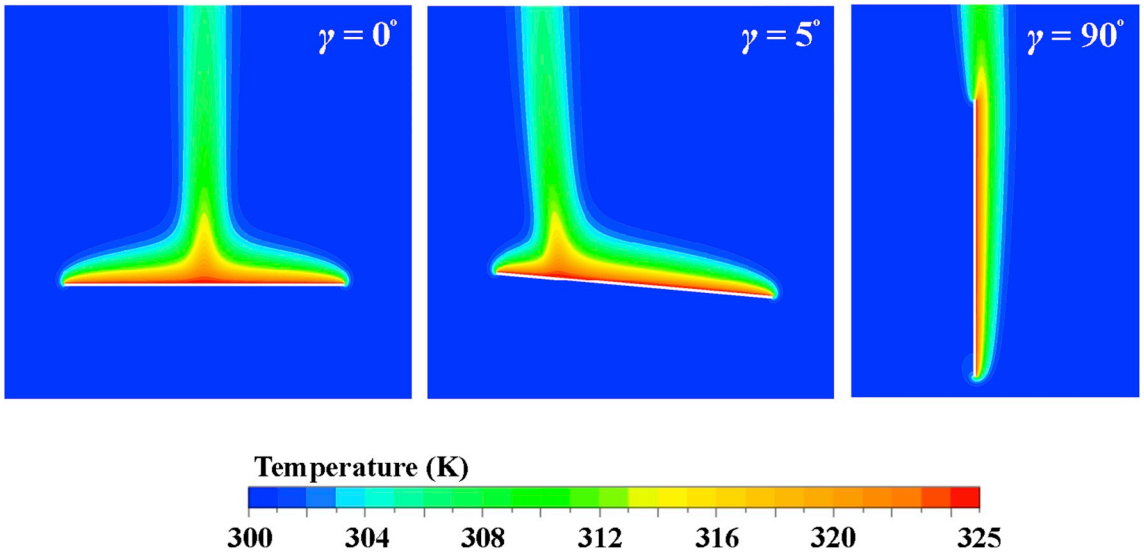

Fig. 4. Contours of temperature at three inclinations for isothermal case: prediction of present CFD simulations (Pr = 0.7, $Gr_L = 10^6$, $T_w - T_\infty = 25$ K).

Table 3
Comparison of Nusselt number obtained by present CFD simulations with experimental results for the isothermal boundary condition.

Rayleigh number Ra_L	Inclination angle γ	Reference no. for experiment	Experimental average Nusselt number $\overline{Nu}$	Average Nusselt number from Present CFD $\overline{Nu}$
7×10^5	90°	[40]	16.00	15.75
7×10^6	90°	[23]	28.00	27.28
Rayleigh number Ra_x			Experimental local Nusselt number Nu_x	Local Nusselt number from Present CFD Nu_x
5×10^5	90°	[25]	10.22	10.31
5×10^5	75°	[25]	9.92	9.99
5×10^5	60°	[25]	9.62	9.69
5×10^5	45°	[25]	9.00	9.14
5×10^5	30°	[25]	8.00	8.19
3×10^6	90°	[23]	17.06	17.54
3×10^6	70°	[23]	16.79	17.27
3×10^6	60°	[23]	16.46	16.92

results from the previous two methods are indicative of that from the present computations though the magnitudes of $\overline{Nu}_t$ obtained from the previous theoretical methods were slightly lower than the values obtained from the present computations. Table 4, however, shows that the values of $\overline{Nu}_t$ determined by the approach of Yu and Lin [27] and that determined by the unified integral method of Guha and Pradhan [2] are significantly different from the values of $\overline{Nu}_t$ determined by CFD in the range $0° \le \gamma \le 15°$. There are two reasons for this difference.

The first reason (which is actually valid over the entire range from 0° to 90°) is that the present method solves the full Navier-Stokes equations in a carefully constructed computational domain and grid, the solutions carried to high level of precision. The semi-analytical formulations use approximate equations. There is a second, more subtle reason for the greater deviations in the range $0° \le \gamma \le 15°$. In the present unified CFD approach, the length scale used in the analysis (for example in defining the Grashof number $Gr_L \equiv [\rho_\infty^2 g\beta(T_w - T_\infty)L^3]/\mu^2$) is taken to be the plate length L at all values of inclination angle γ. The same approach is also taken for the values shown in Table 4 for the entries corresponding to Refs. [2,27]. Equation (14) establishes that the average Nusselt number, $\overline{Nu}_t$, computed through the present CFD solutions is directly indicative of the dependence of the overall heat transfer as a function of the inclination angle. This may not be the case for the values of $\overline{Nu}_t$ computed through the approaches of refs [2,27]. We provide the following physical explanation. Ref [3] established that, for a study of natural convection specifically on a horizontal plate, the most relevant length scale is $L/2$ (since convective boundary layers form on two halves of the plate with a plume in the middle, analytical theories based on semi-infinite assumption can be compared with CFD results up to a maximum limit of $L/2$). Since there is left-right symmetry in the fluid flow field and heat transfer characteristics in the CFD solution for the case of a horizontal plate, the average heat transfer coefficient $\bar{h}$ calculated over any one-half is the same as the arithmetic mean of the $\bar{h}$ values calculated over the left and right halves of the plate. This is not the case for the solutions given by similarity or integral theories which adopt the semi-infinite description. Suppose, these theories predict a total heat transfer rate of $Q_{L,semi-infinite}$ (defined as $\int_0^L q_w dx$) over a plate of length L (where the value of L is fixed by the same value of Gr_L used either in the theories or in the CFD simulation), then the actual total heat transfer rate should be calculated from $Q_{L,corrected} = 2Q_{L/2,semi-infinite}$ (where $Q_{L/2,semi-infinite}$ is the total heat transfer rate through half of the plate starting from the leading edge, given by $\int_0^{L/2} q_w dx$). Using the similarity theory [15], integral theories [2,16] or a more realistic theoretical treatment [3] for a horizontal plate, it can be shown that for the isothermal case q_w is given by $q_w = C/x^{2/5}$, where C is a function of Pr, $(T_w - T_\infty)$ and other properties, but C does not depend on x. Integration of this relation shows that $Q_{L,semi-infinite} = (5/3)CL^{3/5} = k(T_w - T_\infty)\overline{Nu}_{ht,theory}$. Therefore, for a horizontal isothermal plate, the relation between the corrected average

Table 4
Comparison of average Nusselt number obtained by present CFD simulations, numerical analysis, similarity theory and integral analysis for $Gr_L = 10^6$ and Pr = 0.7.

γ (in degree)	$\overline{Nu}_t$(for semi-infinite plate - similarity theory)	$\overline{Nu}_t$(for semi-infinite plate -numerical solution) [27]	$\overline{Nu}_{t,theory}$(for semi-infinite plate - integral analysis) [2]	$\overline{Nu}_{t,corrected}(\equiv F_t\overline{Nu}_t)$ Theoretical $\overline{Nu}_t$ established in the present work	$\overline{Nu}_{t,CFD}$(for finite plate - CFD, present study)
0	9.3589 [15]	9.2685	9.6573	12.7429	12.4953
2.5		9.7210	9.9830	12.7415	12.4610
5		10.2099	10.4284	12.6635	12.4237
7.5		10.6315	10.8451	12.4727	12.3759
10		11.0013	11.2317	12.3191	12.3858
12.5		11.3310	11.5890	12.2703	12.4963
15		11.6286	11.9189	12.2906	12.6704
17.5		11.9460	12.2239	12.3753	12.8774
20		12.1958	12.5062	12.5683	13.0883
22.5		12.4261	12.7681	12.7934	13.2951
25		12.6391	13.0119	13.0119	13.5117
30		12.9686	13.4483	13.4483	13.8999
45		13.8256	14.4420	14.4420	14.8284
60		14.3612	15.0691	15.0691	15.4232
75		14.6456	15.4014	15.4014	15.7248
90	14.875 [4]	14.8750	15.5714	15.5714	15.7503

Table 5
Correction of theoretical average Nusselt number and comparison with CFD result for the isothermal plate ($Gr_L = 10^6$ and Pr = 0.7).

γ degree	$\hat{L}_{RE}$	$\hat{L}_{LE}$	F_t Eqn (17)	$\overline{Nu}_{t,theory}$ Ref [2]	$\overline{Nu}_{t,corrected}$ Eqn (16)	$\overline{Nu}_{t,CFD}$
0	0.5	0.5	$2^{2/5} = 1.319508$	9.6573	12.7429	12.4953
2.5	0.6514	0.3486	1.276321	9.9830	12.7415	12.4610
5	0.7805	0.2195	1.214326	10.4284	12.6635	12.4237
7.5	0.8722	0.1278	1.150080	10.8451	12.4727	12.3759
10	0.9289	0.0711	1.096818	11.2317	12.3191	12.3858
12.5	0.9612	0.0388	1.058791	11.5890	12.2703	12.4963
15	0.9816	0.0184	1.031185	11.9189	12.2906	12.6704
17.5	0.9938	0.0062	1.012383	12.2239	12.3753	12.8774
20	0.9977	0.0023	1.004964	12.5062	12.5683	13.0883
22.5	0.9991	0.0009	1.001981	12.7681	12.7934	13.2951
25	1	0	1	13.0119	13.0119	13.5117
30	1	0	1	13.4483	13.4483	13.8999
45	1	0	1	14.4420	14.4420	14.8284
60	1	0	1	15.0691	15.0691	15.4232
75	1	0	1	15.4014	15.4014	15.7248
90	1	0	1	15.5714	15.5714	15.7503

Nusselt number and the average Nusselt number determined from similarity or integral theories may be established as follows:

$$\overline{Nu}_{ht,corrected} = \frac{2Q_{L/2,semi-infinite}}{k(T_w - T_\infty)} = 2\left(\frac{1}{2}\right)^{3/5} \frac{Q_{L,semi-infinite}}{k(T_w - T_\infty)} = 2^{2/5}\overline{Nu}_{ht,theory} \tag{15}$$

The correction incorporated in equation (15) accounts for the fact that boundary layers grow from both edges of a finite plate. Two further corrections are needed to the boundary layer approach [3], viz. the edge-effect and the alteration of the thermo-fluid-dynamics due to the presence of lift-off point and the plume. Ref [3] gives the details that heat transfer from the wall increases at the edges but decreases underneath the plume. So the combined effect of these two corrections may produce a rather small change in the overall heat transfer rate. Applying the transformation derived above (i.e. equation (15)) to the CFD result for horizontal plate (Table 4), we obtain $12.4953/2^{2/5} = 9.4697$; then the present CFD result comes closer to the previous theoretical values [2,28].

4.1.2. Rationalization for near-horizontal orientations

The transformation for horizontal configuration, equation (15), is rigorously derived. For non-zero values of γ for which significant discrepancy in the theoretical analyses is present (Table 4), however, the exact transformation is not known, and the correspondence between the previous theoretical values and the CFD results cannot be directly established. The corrected value of Nusselt number $\overline{Nu}_{t,corrected}$ (for the isothermal case) can be constructed from,

$$\overline{Nu}_{t,corrected} = F_t \overline{Nu}_{t,theory}, \tag{16}$$

where $\overline{Nu}_{t,theory}$ is the known theoretical value and F_t is a correction factor. $\overline{Nu}_{t,theory}$ may be computed directly from the unified integral theory [2] or from the correlation equation (A3) given in the Appendix. An approximate theoretical treatment for expressing the correction factor F_t as a function of the inclination angle γ is developed below.

Fig. 3 contains the velocity and temperature contours for a value of inclination angle γ in the range $0° < \gamma \leq 15°$. The plume is found to form as two opposite streams moving predominantly parallel to the solid surface transform, at the point of confluence, into a stream moving at right angle to the original streams. The lift-off point is defined as that point where the plume first forms (at which the boundary layers merge) and the distance of that point from the leading (right) edge is called the lift-off distance. Mathematically, the lift-off distance is defined as that particular value of x where the curve of v/u (the ratio which gives the orientation of the overall velocity vector relative to the plate) makes a sharp transition. It is noted that the location of the lift-off point, at which the boundary layers merge into a plume, is not symmetric with respect to two edges of the plate. Let us assume L_{LE} and L_{RE} are the distances of the lift-off point respectively from the left edge and right edge of the plate, as shown in Fig. 3. Taking cue from equation (15), one may write the general expression for the correction factor for the asymmetric location as follows:

$$F_t \equiv \frac{\overline{Nu}_{t,corrected}}{\overline{Nu}_{t,theory}} = (\hat{L}_{LE})^r + (\hat{L}_{RE})^r \tag{17}$$

where, $\hat{L}_{LE}(\equiv L_{LE}/L)$ and $\hat{L}_{RE}(\equiv L_{RE}/L)$ are the corresponding non-dimensional distances, L being the length of the plate. Theories [2] show that the overall heat transfer varies as $L^{3/5}$ for the horizontal plate, and as $L^{3/4}$ for the vertical plate. Using transformations similar to what is used for a validated heat transfer correlation in Ref. [2], it is postulated that

$$r = \frac{3}{5}\cos\gamma + \frac{3}{4}\sin\gamma. \tag{18}$$

Equation (18) shows that when $\gamma = 0°$, $r = 3/5$, and when $\gamma = 90°$, $r = 3/4$. Thus the correct limiting values are obtained. For the horizontal configuration, $\hat{L}_{LE} = \hat{L}_{RE} = 0.5$. Equation (17) then shows that the correction factor reduces to $F_t = 2^{2/5}$, the same implied by equation (15). For the vertical configuration, the right edge of the plate (in our adopted geometry) is the leading edge and the left edge represents the trailing edge; i.e. $\hat{L}_{RE} = 1$, $\hat{L}_{LE} = 0$. Equation (17) then shows that the correction factor reduces to $F_t = 1$. This makes physical sense since, even in the case of a finite plate, a single boundary layer covers the entire length of a vertical plate (i.e. the physical situation is the same as that assumed in the theories for semi-infinite plates).

The values of $\hat{L}_{LE}$ and $\hat{L}_{RE}$ as a function of inclination angle γ are computed in small steps of 2. 5° in the range $0° < \gamma \leq 25°$. Corrected values of average Nusselt number $\overline{Nu}_{t,corrected}$ are therefore calculated as per equations (17) and (18) and are shown in Table 5 and in Fig. 6. Values of $\overline{Nu}_{t,theory}$ shown in Table 5 are calculated by the unified integral theory [2]. The corrected values of the average Nusselt number are reasonably close to the CFD results; moreover $\overline{Nu}_{t,corrected}$ shows the existence of the minimum. Fig. 6 shows the rather dramatic improvement in the theoretical analyses as a result of the introduction of the factor F_t. The utility of F_t is not just in improved predictive power but also in the comprehension of the deviation of the theoretical analyses from reality.

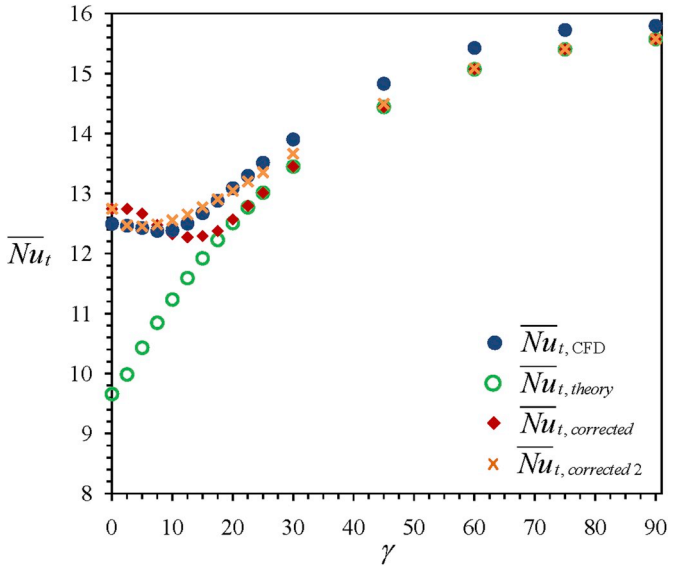

Fig. 6. Variation of average Nusselt number as a function of inclination angle for isothermal plate (at $Gr_L = 10^6$, Pr = 0.7).

It is to be realized that the correction factor F_t addresses only the semi-infinite restriction of the theories but not other restrictions (such as absence of edge effects and plume in the theoretical treatment, use of boundary layer equations, use of non-physical [4] boundary condition such as $u = 0$ at $x = 0$. Ref [3] also discusses the difference between two-dimensional and three-dimensional computations). For inclination angles in which the vertical mechanism of natural convection is dominant [2], $\hat{L}_{LE} = 0$. The edge effects on the leading and trailing edges always increase the local Nusselt number there. For inclination angles where $\hat{L}_{LE} = 0$, the average Nusselt number given by CFD is thus always greater than the theoretical values, even after the application of the correction factor F_t (Fig. 6). For the horizontal and near-horizontal configurations, the additional mechanisms (which are not accounted for in F_t) have opposing effects on the overall heat transfer. The edge effects increase the heat transfer whereas there is a reduction in heat transfer underneath the plume. $\overline{Nu}_{t,corrected}$ can thus be above or below $\overline{Nu}_{t,CFD}$ for the horizontal and near-horizontal configurations (Fig. 6).

A simpler approach for the correction factor for isothermal case, $F_{t,2}$, is postulated below,

$$F_{t,2} \equiv \frac{\overline{Nu}_{t,corrected2}}{\overline{Nu}_{t,theory}} = 1 + \left(2^{2/5} - 1\right)\exp\left(-\gamma/\gamma_m\right), \tag{19}$$

where, γ_m is a constant (whose value may depend on the Grashof number and Prandtl number). The form of the correction factors $F_{t,2}$ is based on the fact that the required semi-infinite correction is the greatest for $\gamma = 0°$ and that the correction should reduce to zero for $\gamma = 90°$. Moreover, the correction is expected to change rapidly as γ increases from zero, since the present investigation shows that the lift-off point shifts toward the trailing edge rapidly with increasing γ in the near-horizontal positions. Thus the exponential function in equation (19) is postulated to account for the expected limiting values ($F_{t,2} = 2^{2/5}$ at $\gamma = 0°$ and $F_{t,2} \approx 1$ at $\gamma = 90°$) and sensitivity at small γ. The appropriateness of the postulation can be judged from the acceptability of its predictions. The prediction of equation (19) is also included in Fig. 6 with $\gamma_m = 10°$. The comparison with the CFD curve is reasonable. An advantage of equation (19) over (17) is that any knowledge about the location of the lift-off point is not required, and equation (19) can therefore be used without any a priori knowledge, but the formulation is postulatory.

Table 5 and Fig. 6 show that, for an isothermally heated plate, there is significant difference between the average Nusselt number (hence the overall heat transfer rate) for the horizontal and vertical orientation of the plate. For example, at $Gr_L = 10^6$ and Pr = 0.7, $\overline{Nu}_{ht} = 12.4953$ and $\overline{Nu}_{vt} = 15.7941$, i.e. the overall heat transfer rate from a plate of finite length would increase by more than 25% if the orientation of the plate is changed from the horizontal to the vertical. This trend is maintained at other values of Grashof number also. For example, when the present CFD simulations are run at $Gr_L = 10^7$ and Pr = 0.7, it is found that $\overline{Nu}_{ht} = 19.7297$ and $\overline{Nu}_{vt} = 27.2746$, i.e. the increase is more than 35%.

4.2. Natural convection around heated inclined plates for constant heat flux condition

Several CFD simulations are run here for another surface boundary condition, viz., the constant heat flux boundary condition for the sake of completeness. Such additional computations show that although the numerical values of the various parameters such as the Nusselt number are slightly different from their isothermal counterparts, the broad physical picture of natural convective heat transfer, the physics of entrainment, and the evolution of the buoyant jet remain essentially the same. Therefore a brief theoretical study at various inclination angles is reported below. The definition of Grashof number needs to be changed from the isothermal case. The modified local Grashof number Gr_x^* is defined as $Gr_x^* = (\rho_\infty^2 g\beta q_w x^4)/(k\mu^2)$. The modified Grashof number based on the plate length L is therefore given by $Gr_L^* = (\rho_\infty^2 g\beta q_w L^4)/(k\mu^2)$.

Figs. 7 and 8 respectively show the computed velocity and temperature contours for an assumed constant surface heat flux of $q_w = 100\ \mathrm{W/m^2}$ in a fluid with Pr = 0.7. All parameters including the plate length are kept at the same values as mentioned for the isothermal study, only the values of k and μ are adjusted to obtain the modified Grashof number as $Gr_L^* = 10^6$. The contours of velocity for three inclination angles in the range $0° \le \gamma \le 90°$ are shown in Fig. 7. The general characteristics of the velocity field in the vicinity of the plate subjected to constant heat flux remain similar to those observed for the isothermal case (Fig. 3).

There is an important difference in the general characteristics of the temperature field between the isothermal case (Fig. 4) and the constant heat flux case (Fig. 8). While the surface temperature for the heated side of the plate was kept fixed (at T_w) in the isothermal case, the value of T_w varies along the length of the plate for the constant heat flux case (Fig. 8). This is reflected in the distribution of the fluid temperature inside the convective boundary layer. However, the tendency of the

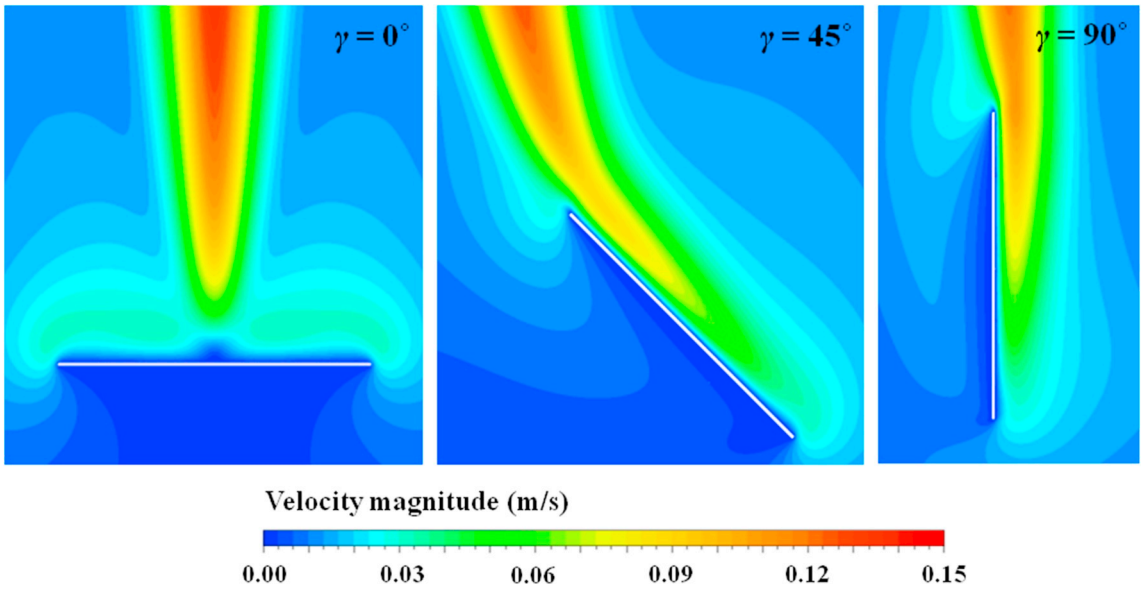

Fig. 7. Contours of velocity magnitude at three inclinations for constant wall heat flux case: prediction of present CFD simulations (Pr = 0.7, $Gr_L^* = 10^6$, $q_w = 100\ \mathrm{W/m^2}$).

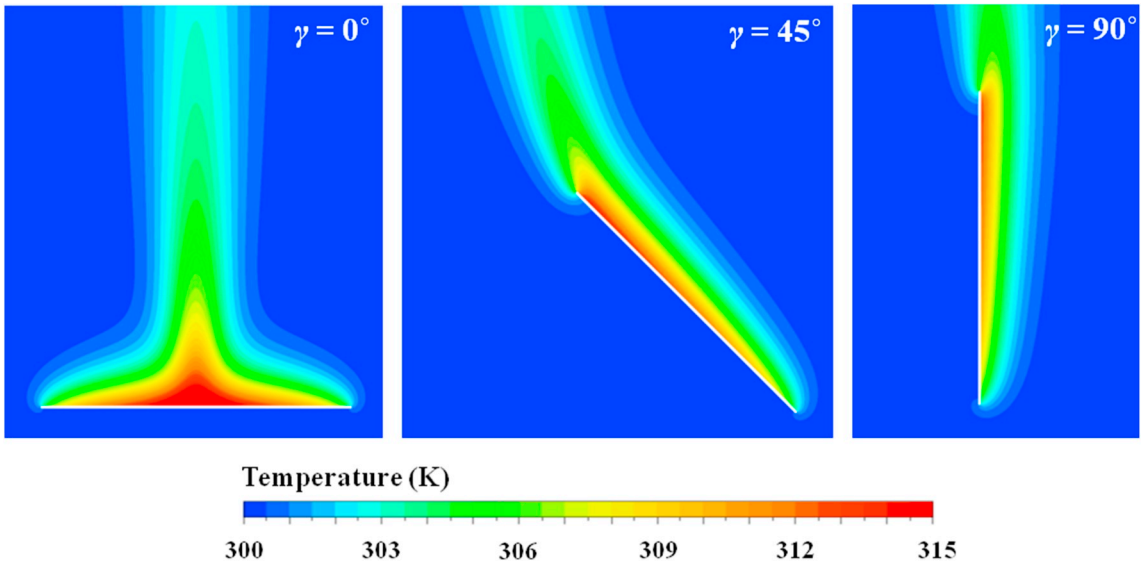

Fig. 8. Contours of temperature at three inclinations for constant wall heat flux case: prediction of present CFD simulations (Pr = 0.7, $Gr_L^* = 10^6$, q_w = 100 W/m^2).

temperature inside the buoyant plume to decrease with vertical distance from the plate that is observed for the isothermal case prevails here as well.

When the plate surface heat flux is constant, the surface temperature varies along the x-direction. The computed variation in plate surface temperature (in non-dimensional form) is shown in Fig. 9 for three inclination angles. Each curve passes through a maximum point ($T_{w,\max}$) whose location shifts from the centre of the plate for the horizontal orientation ($\gamma = 0°$) to near the trailing edge for the vertical ($\gamma = 90°$). It is observed that the value of $T_{w,\max}$ decreases as the orientation of the plate is changed from the horizontal to the vertical. However, the rate of decrease of $T_{w,\max}$ as well as the rate of shift of the maximum decreases with increasing values of γ. The principal reason for the existence of the maximum surface temperature point may change depending on the inclination angle. For the horizontal and near-horizontal positions, where the buoyant plume forms within the heated side of the plate, reduced heat transfer underneath the plume (due to uplifting of the fluid as a result of confluence of two oppositely moving streams) is responsible for the rise of wall temperature (q_w remaining the same at all points on the wall). However, for such orientations of the plate where the vertical mechanism of natural convection is dominant [2], the wall temperature steadily increases toward the trailing edge due to the continuous thickening of the boundary layer (the wall heat flux q_w remaining constant) until a point is reached close to the trailing edge where edge-effects increase the heat transfer rate (with associated decrease of wall temperature). The maxima shown for $\gamma = 0°$ and $\gamma = 5°$ occur due to the first effect, while the maxima shown for $\gamma = 45°$ and $\gamma = 90°$ exist due to the second effect.

A comparison of Figs. 5 and 9 shows that the heat flux profiles for isothermal case exhibit inverse relation with the surface temperature profiles for constant heat flux case. The locations of low surface heat flux in Fig. 5 correspond to those of high surface temperature in Fig. 9 and vice versa.

Table 6 shows a few experimental values of local Nusselt number and the corresponding values determined from the present CFD method at various values of modified Raleigh number ($Ra_x^* = Gr_x^* \mathrm{Pr}$) given in the experiments. The agreement is good.

4.2.1. Determination of average Nusselt number

As a result of the variable wall temperature, caution (and consistency) is needed in the determination of average Nusselt number which, for the constant heat flux case, is denoted here by $\overline{Nu}_q$. The following formulation for $\overline{Nu}_q$ is used here (other definitions have also been used in the literature [41]):

$$\overline{Nu}_q = \frac{\bar{h}L}{k} = \frac{L}{k}\frac{1}{L}\int_0^L h dx = \frac{q_w}{k}\int_0^L \frac{1}{(T_w - T_\infty)} dx. \tag{20}$$

Table 7 shows the present CFD results for $\overline{Nu}_q$ vis-à-vis the values of $\overline{Nu}_q$ that can be computed by integrating the results for Nu_x given in two previous theoretical work [2,28]. Yu and Lin [28] had numerically solved, by finite-difference method, the boundary layer equations for natural convection around a semi-infinite heated inclined plate, using a complex co-ordinate transformation. Guha and Pradhan [2] formulated a unified integral theory for arbitrary inclination, in which the orders of polynomial representing the velocity and temperature profiles could be optimized. For accurate determination of the Nusselt number, a large number of grid points, approximately 0.7–0.9 million points depending on the inclination angle, is used in the present CFD simulations.

4.2.2. Correction factor for constant-heat-flux horizontal plate

It is recognized that the main difference between the semi-infinite approach assumed in the integral theory and the treatment of finite plate in CFD (and experiments) is that boundary layers grow from both

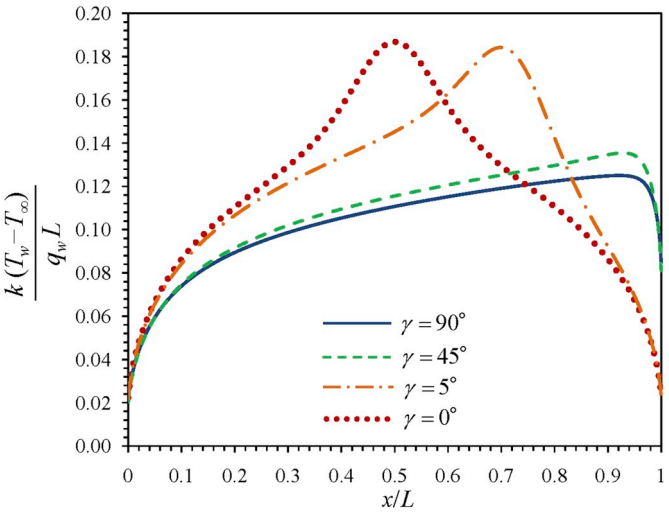

Fig. 9. Variation of non-dimensional surface temperature along the heated side of the plate at various angles of inclination in the range $0° \le \gamma \le 90°$ (at $Gr_L^* = 10^6$, Pr = 0.7).

Table 6
Experimental validation of present CFD results at various angles of inclination for the constant heat flux boundary condition.

Ra_x^*	γ(in degree)	Nu_x Experimental value (ref no. is given within bracket)	Nu_x Present CFD results
0.7×10^6	90	11.55 [10]	11.77
4.97×10^6	60	12.73 [24]	12.61
4.97×10^6	45	12.24 [24]	12.15
4.97×10^6	30	11.41 [24]	11.41

Table 7
Comparison of average Nusselt number obtained by present CFD simulations, numerical analysis, similarity theory and integral analysis ($Gr_L^* = 10^6$ and Pr = 0.7).

γ(in degree)	$\overline{Nu}_q$(for semi-infinite plate - similarity theory)	$\overline{Nu}_q$(for semi-infinite plate -numerical solution) [28]	$\overline{Nu}_{q,theory}$(for semi-infinite plate - integral analysis) [2]	$\overline{Nu}_{q,CFD}$(for finite plate - CFD, present study)
0	7.8238 [15]	7.8109	7.6179	9.7017
2.5		7.8848	7.7252	9.6512
5		8.1060	7.8972	9.5283
7.5		8.2931	8.0575	9.2450
10		8.4537	8.2068	8.9984
12.5		8.5945	8.3457	8.9864
15		8.7194	8.4749	9.0157
17.5		8.8314	8.5953	9.0820
20		8.9324	8.7074	9.1638
25		9.1071	8.9090	9.3648
30		9.2515	9.0839	9.5746
45		9.5439	9.4755	9.9834
60		9.6642	9.7026	10.2414
75		9.6252	9.7852	10.3370
90	9.5769 [42]	9.5497	9.7569	10.3027

edges of a finite horizontal plate and there is a plume at the middle. Table 7 shows (in line with the isothermal case dealt with in Section 4.1) that, for $\gamma = 0°$, there is a large discrepancy in the average Nusselt number calculated by CFD and that calculated from theories based on the semi-infinite assumption. In order to rectify this deficiency, we first calculate the average heat transfer coefficient $\bar{h}_{L/2}$ between the leading edge and the mid-point of the plate. The formulation given in Ref. [16] shows that for the constant-heat-flux case the local heat transfer coefficient h_x is given by $h_x = C/x^{1/3}$, where C is a function of Pr, q_w and other properties, but C does not depend on x. Integration of this equation shows that $\bar{h}_{L/2} = \frac{2}{L}\int_0^{L/2} h_x dx = \frac{2}{L}C\frac{3}{2}(L/2)^{2/3} = (2/2^{2/3})\frac{1}{L}\int_0^{L} h_x dx = 2^{1/3}\bar{h}_L$. The corrected average Nusselt number for a horizontal plate for constant heat flux case then becomes,

$$\overline{Nu}_{hq,corrected} = \frac{\bar{h}_{L/2}L}{k} = 2^{1/3}\frac{\bar{h}_L L}{k} = 2^{1/3}\overline{Nu}_{hq,theory} \tag{21}$$

where, $\overline{Nu}_{q,theory}$ shown in Table 7 is computed by using the unified integral theory [2]. Applying the transformation derived above (i.e. equation (21)) to the CFD result for horizontal plate (Table 7), we obtain $9.7017/2^{1/3} = 7.7002$; then the present CFD result comes closer to the previous theoretical values [2,28].

4.2.3. Correction factor for non-zero inclination angles with focus on near-horizontal orientations

Table 7 shows that the difference of average Nusselt number between the horizontal and vertical configurations for the constant-heat-flux case is rather modest, as compared to the isothermal case. On the other hand, for the range of inclination angle $0° < \gamma \leq 15°$, while we had concluded for the isothermal case that the flow field changes drastically but the variation in average Nusselt number is modest (Table 4), Table 7 shows that the change in average Nusselt number for the constant-heat-flux case is more significant. There exists a minimum in average Nusselt number both in the isothermal and constant heat flux cases.

The corrected value of Nusselt number $\overline{Nu}_{q,corrected}$ (for constant-heat-flux case) can be constructed from,

$$\overline{Nu}_{q,corrected} = F_q \overline{Nu}_{q,theory}, \tag{22}$$

where $\overline{Nu}_{q,theory}$ is the known theoretical value which may be computed directly from the unified integral theory [2] or from the correlation equation (A6) given in the Appendix. An approximate theoretical treatment for expressing the correction factor F_q as a function of the inclination angle γ is developed below.

Figs. 10 and 11 contain respectively the velocity and temperature contours for three values of inclination angle γ in the range $0° < \gamma \leq 15°$. It is noted that the location of the lift-off point, at which the boundary layers merge into a plume, is not symmetric with respect to two edges of the plate. Let us assume L_{LE} and L_{RE} are the distances of

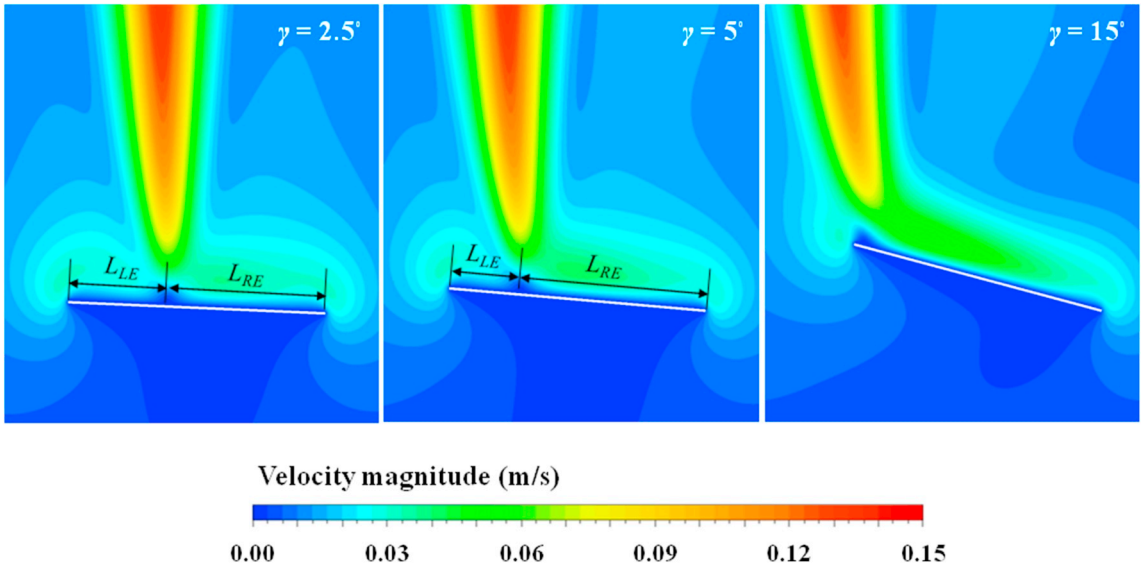

Fig. 10. Contours of velocity magnitude at three near-horizontal positions for constant wall heat flux case: prediction of present CFD simulations (Pr = 0.7, $Gr_L^* = 10^6$, $q_w = 100$ W/m^2).

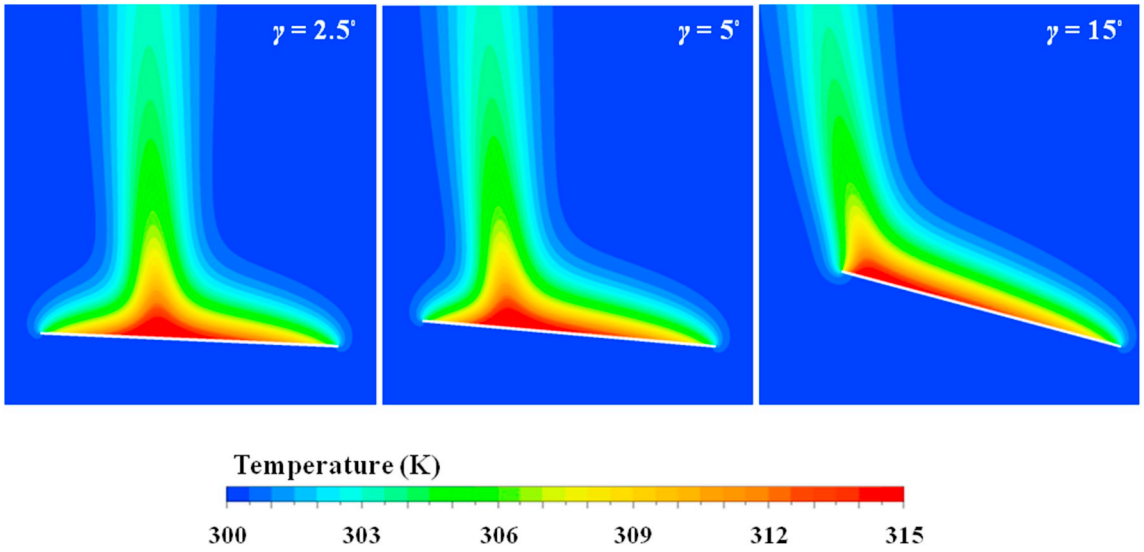

Fig. 11. Contours of temperature at three near-horizontal positions for constant wall heat flux case: prediction of present CFD simulations (Pr = 0.7, $Gr_L^* = 10^6$, $q_w = 100\ \mathrm{W/m^2}$).

the lift-off point respectively from the left edge and right edge of the plate, as shown in Fig. 10. Following the methodology for the isothermal case (Section 4.1.2), one may write the general expression for the correction factor for the asymmetric location as follows:

$$F_q \equiv \frac{\overline{Nu}_{q,corrected}}{\overline{Nu}_{q,theory}} = (\hat{L}_{LE})^{rq} + (\hat{L}_{RE})^{rq} \tag{23}$$

where, $\hat{L}_{LE}(\equiv L_{LE}/L)$ and $\hat{L}_{RE}(\equiv L_{RE}/L)$ are the corresponding non-dimensional distances, L being the length of the plate. Relations given in the Appendix show that the average Nusselt number varies as $L^{2/3}$ for the horizontal plate, and as $L^{4/5}$ for the vertical plate. Using transformations similar to what is used for a validated heat transfer correlation in Ref. [2], it is postulated that

$$rq = \frac{2}{3}\cos\gamma + \frac{4}{5}\sin\gamma. \tag{24}$$

Equation (24) shows that when $\gamma = 0°$, $rq = 2/3$, and when $\gamma = 90°$, $rq = 4/5$. Thus the correct limiting values are obtained. For the horizontal configuration, $\hat{L}_{LE} = \hat{L}_{RE} = 0.5$. Equation (23) then shows that the correction factor reduces to $F_q = 2^{1/3}$, the same implied by equation (21). For the vertical configuration, the right edge of the plate (in our adopted geometry) is the leading edge and the left edge represents the trailing edge; i.e. $\hat{L}_{RE} = 1$, $\hat{L}_{LE} = 0$. Equation (23) then shows that the correction factor reduces to $F_q = 1$. This makes physical sense since, even in the case of a finite plate, a single boundary layer covers the entire length of a vertical plate (i.e. the physical situation is the same as that assumed in the theories for semi-infinite plates).

The values of $\hat{L}_{LE}$ and $\hat{L}_{RE}$ as a function of inclination angle γ are computed for the constant wall heat flux case in the present work, in small steps of 2. 5° in the range $0° < \gamma \leq 25°$. Corrected values of average Nusselt number $\overline{Nu}_{q,corrected}$ are therefore calculated as per equations (23) and (24) and are shown in Table 8 and in Fig. 12. Values of $\overline{Nu}_{q,theory}$ shown in Table 8 are calculated by the unified integral theory [2]. The corrected values of the average Nusselt number are reasonably close to the CFD results; moreover $\overline{Nu}_{q,corrected}$ shows the existence of the minimum. Fig. 12 shows the rather dramatic improvement in the theoretical analyses as a result of the introduction of the factor F_q. The utility of F_q is not just in improved predictive power but also in the comprehension of the deviation of the theoretical analyses from reality.

It is to be realized that the correction factor F_q addresses only the semi-infinite restriction of the theories but not other restrictions (such as absence of edge effects and plume in the theoretical treatment, use of boundary layer equations, use of non-physical [4] boundary condition

Table 8
Correction of theoretical average Nusselt number and comparison with CFD result for the constant wall heat flux case ($Gr_L^* = 10^6$ and Pr = 0.7).

γ degree	$\hat{L}_{RE}$ Present CFD	$\hat{L}_{LE}$ Present CFD	F_q Eqn (23)	$\overline{Nu}_{q,theory}$ Ref [2]	$\overline{Nu}_{q,corrected}$ Eqn (22)	$\overline{Nu}_{q,CFD}$ Present CFD
0	0.5	0.5	$2^{1/3} = 1.259921$	7.6179	9.5980	9.7017
2.5	0.3875	0.6125	1.223739	7.7252	9.4536	9.6512
5	0.2715	0.7285	1.176703	7.8972	9.2927	9.5283
7.5	0.1825	0.8175	1.129085	8.0575	9.0976	9.2450
10	0.1145	0.8855	1.086171	8.2068	8.9140	8.9984
12.5	0.0775	0.9225	1.057243	8.3457	8.8234	8.9864
15	0.0475	0.9525	1.034224	8.4749	8.7649	9.0157
17.5	0.0217	0.9783	1.0158	8.5953	8.7311	9.0820
20	0.0061	0.9939	1.004662	8.7074	8.7480	9.1638
25	0.0007	0.9993	1.000405	8.9090	8.9126	9.3648
30	0	1	1	9.0839	9.0839	9.5746
45	0	1	1	9.4755	9.4755	9.9834
60	0	1	1	9.7026	9.7026	10.2414
75	0	1	1	9.7852	9.7852	10.3370
80	0	1	1	9.7812	9.7812	10.3413
85	0	1	1	9.7608	9.7608	10.3279
90	0	1	1	9.7569	9.7569	10.3027

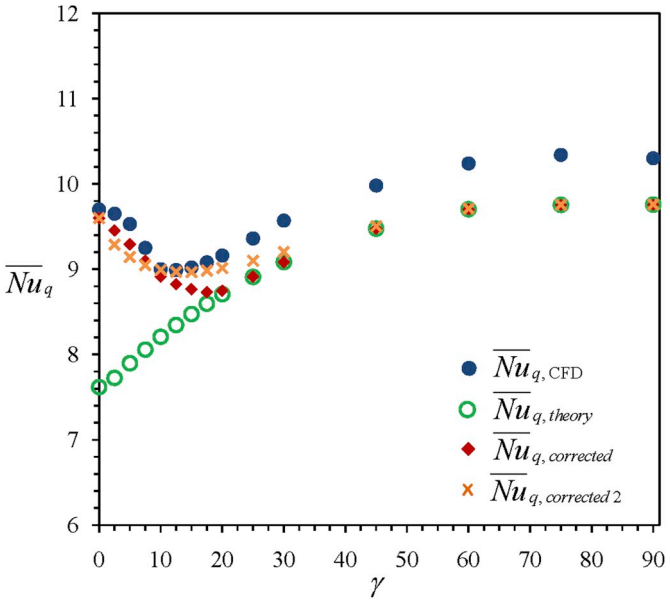

Fig. 12. Variation of average Nusselt number as a function of inclination angle for constant wall heat flux (at $Gr_L^* = 10^6$, Pr = 0.7).

such as $u = 0$ at $x = 0$. Ref [3] also discusses the difference between two-dimensional and three-dimensional computations). For inclination angles in which the vertical mechanism of natural convection is dominant [2], $\hat{L}_{LE} = 0$. The edge effects on the leading and trailing edges always increase the local Nusselt number there. For inclination angles where $\hat{L}_{LE} = 0$, the average Nusselt number given by CFD is thus always greater than the theoretical values, even after the application of the correction factor $F_{\bar{q}}$ (Fig. 12). For the horizontal and near-horizontal configurations, the additional mechanisms (which are not accounted for in $F_{\bar{q}}$) have opposing effects on the overall heat transfer. The edge effects increase the heat transfer whereas there is a reduction in heat transfer underneath the plume. Fig. 12 shows that the increase due to edge effects exceeds the reduction due to the presence of the plume, and $\overline{Nu}_{q,CFD}$ is generally greater than $\overline{Nu}_{q,corrected}$ even for the horizontal and near-horizontal configurations. This is subtly different from the behaviour of relative magnitudes of $\overline{Nu}_{t,CFD}$ and $\overline{Nu}_{t,corrected}$ shown in Fig. 6.

A simpler approach for the correction factor for the constant-heat-flux case, $F_{\bar{q},2}$, is postulated below,

$$F_{\bar{q},2} \equiv \frac{\overline{Nu}_{q,corrected\,2}}{\overline{Nu}_{q,theory}} = 1 + (2^{1/3} - 1)\exp(-\gamma/\gamma_m). \tag{25}$$

The rationale for the postulation contained in equation (25) is similar to that given after equation (19), and its appropriateness can be judged from the acceptability of its predictions. According to equation (25), $F_{\bar{q},2}$ reduces to the correct limiting value at $\gamma = 0°$ compatible to equation (21) which is rigorously derived. For the vertical configuration, i.e. at $\gamma = 90°$, equation (25) gives $F_{\bar{q},2} \approx 1$ which corresponds to physical reality as explained in Section 4.1.2. The prediction of equation (25) is also included in Fig. 12 with $\gamma_m = 10°$. The comparison with the CFD curve is reasonable. An advantage of equation (25) over (23) is that any knowledge about the location of the lift-off point is not required, and equation (25) can therefore be used without a priori knowledge, but the formulation is postulatory.

4.2.4. Behaviour of $\overline{Nu}_q$ in near-vertical orientations

Table 4 for the isothermal case shows that $\overline{Nu}_t$ changes significantly as the inclination angle γ is increased from 15° to 60°, and the $\overline{Nu}_t$ versus γ curve continues to rise (though slowly) in the range $60° < \gamma < 90°$. Table 7 shows that $\overline{Nu}_{q,CFD}$ is quite flat in the range $60° < \gamma < 90°$ and an additional feature is noticed that there exists a small maximum at about

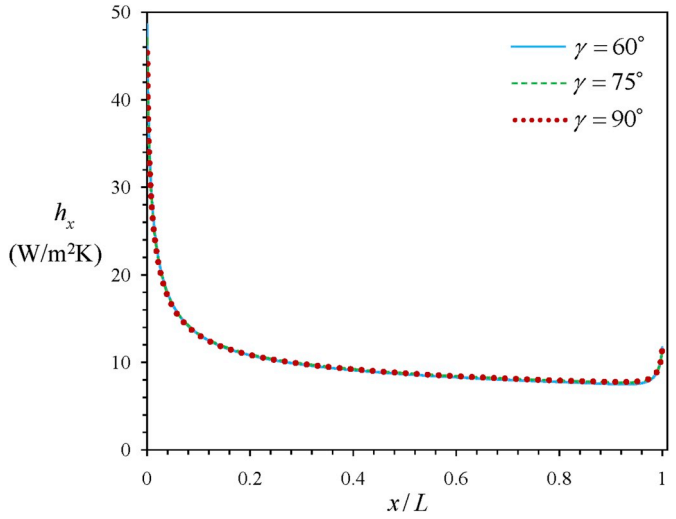

Fig. 13. Variation of local heat transfer coefficient along the length of a finite plate in near-vertical orientations for constant wall heat flux (at $Gr_L^* = 10^6$, Pr = 0.7).

$\gamma = 80°$. Since great care is taken in the present CFD simulations to attain high accuracy in the computed values of the Nusselt number, further investigation is carried out, the details of which are shown in Fig. 13, Fig. 14 and Table 9. Fig. 13 shows that the h_x versus $\bar{x}$ distributions at various angles of inclination in the range $60° < \gamma < 90°$ nearly coincide with each other on the scale of the graph. There are three regions in the distribution. Close to the leading edge, the value of h_x is the highest ($h_x|_{x=0}$) and it then sharply decreases with increasing $\bar{x}$. In the middle of the plate, h_x slowly decreases with increasing $\bar{x}$, thereby reaching a minimum value ($h_{x,\min}$). In the third region close to the trailing edge, h_x sharply increases with increasing $\bar{x}$, thereby reaching a value $h_x|_{x=L}$ which, although much greater than the heat transfer rate in the middle, is always found to be less than the value at the leading edge ($h_x|_{x=0} > h_x|_{x=L}$). The variation of $h_x|_{x=0}$, $h_{x,\min}$ and $h_x|_{x=L}$ as a function of inclination angle γ is shown in Fig. 14. The extents in $\bar{x}$ of the regions in which h_x for a given inclination angle is greater or less than the h_x at the same $\bar{x}$ location for a vertical plate, determined by the present CFD, are given in Table 9.

A detailed study of Fig. 14 and Table 9 highlights the subtle dependence of the three heat transfer regions on the inclination angle for a finite plate in the near-vertical orientations that causes the existence a small maximum in $\overline{Nu}_{q,CFD}$ at about $\gamma = 80°$ (at $Gr_L^* = 10^6$, Pr = 0.7). It

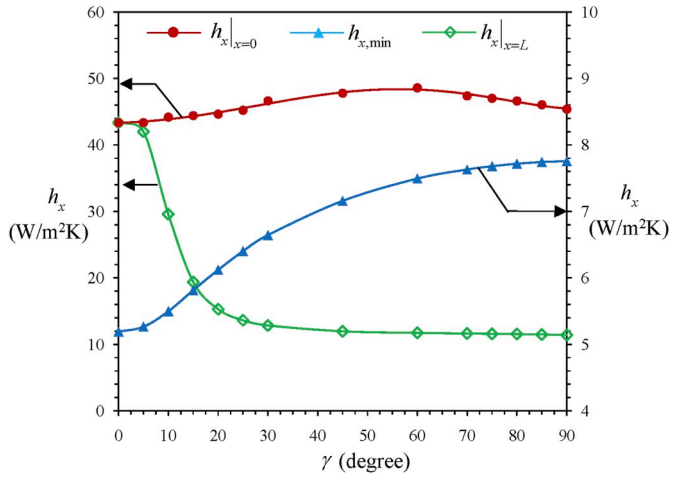

Fig. 14. Variation of minimum and maximum heat transfer coefficients as a function of the plate inclination angle for constant wall heat flux (at $Gr_L^* = 10^6$, Pr = 0.7).

Table 9
Analysis of the variation of heat transfer coefficient along the plate length as a function of the plate inclination angle: results of present CFD ($Gr_L^* = 10^6$ and Pr = 0.7).

γ degree	Range of $\bar{x}$ near leading edge over which h_x is greater than its corresponding value for $\gamma = 90°$	Range of $\bar{x}$ in the middle of the plate over which h_x is less than its corresponding value for $\gamma = 90°$	Range of $\bar{x}$ near trailing edge over which h_x is greater than its corresponding value for $\gamma = 90°$
25	n/a	0–0.98613	0.98613–1
30	0–0.01387	0.01387–0.9897	0.9897–1
45	0–0.06	0.06–0.99294	0.99294–1
60	0–0.164	0.164–0.99232	0.99232–1
70	0–0.343	0.343–0.99104	0.99104–1
75	0–0.497	0.497–0.9897	0.9897–1
80	0–0.794	0.794–0.98537	0.98537–1
85	0–0.824	0.824–0.98537	0.98537–1

is noted that, at $\gamma = 80°$, the leading edge region in which $h_x > h_x(\gamma = 90°)$ extends beyond three-fourth of the plate ($\bar{x} = 0.794$), and

$h_x|_{x=0}\ (\gamma = 80°) - h_x|_{x=0}\ (\gamma = 90°) > h_{x,\min}\ (\gamma = 90°) - h_{x,min}\ (\gamma = 80°)$.

The data in the third column of Table 7 shows the existence of a small maximum in $\overline{Nu}_q$ at $\gamma = 60°$; however, one should not over-interpret this aspect. These values of $\overline{Nu}_q$ have been computed here by integrating the results for Nu_x given in a previous theoretical work [28]. Yu and Lin [28] had numerically solved, by finite-difference method, the boundary layer equations for natural convection around a semi-infinite heated inclined plate, using a complex co-ordinate transformation. As a result of the used multi-layered complex transformation, it is found that when the data are expressed in terms of usual variables, there are not enough data points in large ranges of x and γ. Consequently, the corresponding numerical integration to determine $\overline{Nu}_q$ is expectedly not carried out to the same level of precision with which $\overline{Nu}_{q,CFD}$ is determined in the present work. The values of $\overline{Nu}_q$ given in the fourth column of Table 7 shows the existence of a small maximum at $\gamma = 75°$, which nearly coincides with the conclusion from the CFD simulations. Although the strength of the unified theory of Guha and Pradhan [2] is now well established, such coincidence still seems to be a bit surprising since the values of Nu_x near the leading edge of the plate are responsible for the existence of the maximum in $\overline{Nu}_q$ and any boundary layer based theory has its limitation close to the leading edge.

4.3. Dependence of average Nusselt number on the boundary condition

Fig. 15 sheds light on the influence of the boundary condition - isothermal versus iso-wall-heat-flux - on the average Nusselt number for natural convection around a heated finite plate ($Gr_L = Gr_L^* = 10^6$, Pr = 0.7). At all inclinations, the isothermal case gives greater average Nusselt number ($\overline{Nu}_t > \overline{Nu}_q$, for $Gr_L = Gr_L^*$). The average Nusselt number in the vertical orientation is greater than that for the horizontal orientation of the same finite plate. The difference in Nusselt number between the vertical and the horizontal orientation is greater for the isothermal case ($\overline{Nu}_{vt} - \overline{Nu}_{ht} > \overline{Nu}_{vq} - \overline{Nu}_{hq}$). However, in the near-horizontal positions, the variation in the average Nusselt number with inclination angle is more prominent for the constant wall heat flux boundary condition. The minimum in $\overline{Nu}_t$ for isothermal plate (at $Gr_L = 10^6$, Pr = 0.7) occurs around $\gamma = 7.5°$, while the minimum in $\overline{Nu}_q$ for the iso-wall-heat-flux plate (at $Gr_L^* = 10^6$, Pr = 0.7) occurs around $\gamma = 12.5°$.

The rather small range of average Nusselt number for the constant wall heat flux case is demonstrated here at $Gr_L^* = 10^6$ and Pr = 0.7; for which $\overline{Nu}_{hq} = 9.7017$ and $\overline{Nu}_{vq} = 10.3027$, i.e. the overall heat transfer rate from a plate of finite length would increase only by 6% if the orientation of the plate is changed from the horizontal to the vertical. This trend is maintained at other values of modified Grashof number also. For example, when the present CFD simulations are run at $Gr_L^* = 10^7$ and Pr = 0.7 it is found that $\overline{Nu}_{hq} = 14.3689$ and $\overline{Nu}_{vq} = 15.9402$, i.e. the range in average Nusselt number remains modest.

4.4. Correction factor at varying Grashof and Prandtl numbers

The correction factors discussed in this paper address the semi-infinite restriction of the theories but not other restrictions (such as absence of edge effects and plume in the theoretical treatment, use of boundary layer equations, and use of non-physical [4] boundary condition such as $u = 0$ at $x = 0$ in the theories). In Tables 4, 5 and 8, and in Figs. 6, 12 and 15, we have studied the effects of varying inclination angle γ on the average Nusselt number $\overline{Nu}$ for isothermal and iso-heat-flux conditions while keeping the Grashof and Prandtl numbers fixed ($Gr_L = Gr_L^* = 10^6$Pr = 0.7). In this section, we examine the effect of varying Grashof and Prandtl numbers on $\overline{Nu}$ for the horizontal orientation of the plate (i.e. γ is fixed at 0°). For this purpose, a number of additional CFD simulations are performed to high degree of precision at various combinations of Grashof and Prandtl numbers for both boundary conditions. 10 additional values of $\overline{Nu}$ thus computed are given in Table 10, along with the results discussed in previous Sections. Values of $\overline{Nu}$ determined by similarity theory [15] and integral theory [2,16] for the same combinations of Grashof and Prandtl numbers are also included in Table 10. Relevant equations for these theories are given in the Appendix for ready reference.

An approximate range of Grashof numbers is selected in Table 10,

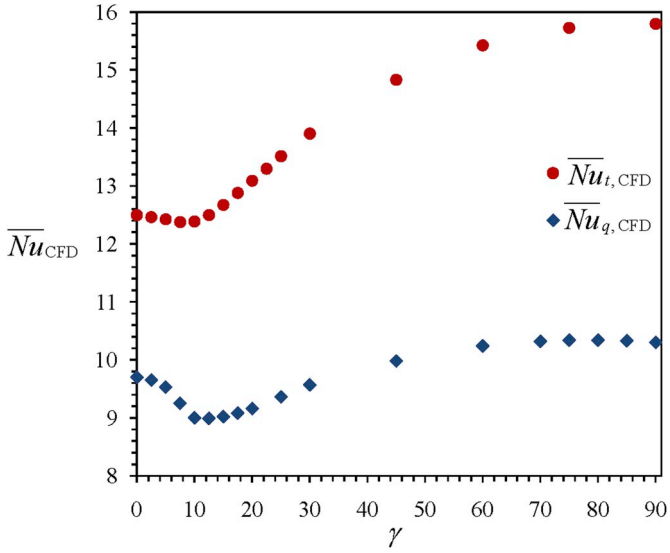

Fig. 15. Variation of average Nusselt number as a function of inclination angle for finite plates with constant surface temperature and constant wall heat flux: prediction of present CFD simulations ($Gr_L = Gr_L^* = 10^6$, Pr = 0.7).

Table 10
Demonstration that the semi-infinite correction factors $F_t = 2^{2/5}$ and $F_q = 2^{1/3}$ for the horizontal orientation of the heated plate are independent of the Grashof and Prandtl numbers.

Isothermal horizontal plate

Gr_L	Pr	$\overline{Nu}_{ht}$(for semi-infinite plate - similarity theory) Eqn (A7)	$\overline{Nu}_{ht,theory}$(for semi-infinite plate - integral analysis) Eqn (A2)	$2^{2/5}\,\overline{Nu}_{ht,theory}$	$\overline{Nu}_{ht,CFD}$(for finite plate - CFD, present study)
10^5	0.7	5.9051	6.0934	8.0402	7.8942
10^6	0.7	9.3589	9.6573	12.7429	12.4953
10^7	0.7	14.8329	15.3059	20.1962	19.7297
10^5	10	11.2841	11.3438	14.9683	15.8474
10^6	10	17.8841	17.9788	23.7231	24.3467
10^7	10	28.3444	28.4944	37.5986	37.9710

Iso-heat-flux horizontal plate

Gr_L^*	Pr	$\overline{Nu}_{hq}$(for semi-infinite plate - similarity theory) Eqn (A8)	$\overline{Nu}_{hq,theory}$(for semi-infinite plate - integral analysis) Eqn (A5)	$2^{1/3}\,\overline{Nu}_{hq,theory}$	$\overline{Nu}_{hq,CFD}$(for finite plate - CFD, present study)
10^5	0.7	5.3303	5.1900	6.5390	6.3955
10^6	0.7	7.8238	7.6179	9.5980	9.7017
10^7	0.7	11.4838	11.1816	14.0879	14.3693
10^5	10	8.9810	8.8477	11.1474	12.3039
10^6	10	13.1823	12.9866	16.3621	17.4526
10^7	10	19.3490	19.0617	24.0163	24.9905

where the lower bound is controlled by the appropriateness of the assumption of a boundary layer type flow and the upper bound is controlled by the appropriateness of the assumption of laminar flow [3]. The two selected values of Prandtl number in the limited parametric study shown in Table 10 are indicative of the natural convection in two most common fluids - air and water. It is possible to run additional CFD simulations at varying inclination angles γ for the combinations of Grashof and Prandtl numbers given in Table 10 (or at any other relevant combination). The appropriate values of $\hat{L}_{LE}$ and $\hat{L}_{RE}$ in equations (17) and (23), and that of γ_m in equations (19) and (25) for the particular combination can then be determined following the methodology established in this paper.

The mathematical deduction procedures leading to equations (15) and (21) reveal that the correction factors for the horizontal plate ($F_t = 2^{2/5}$ for the isothermal and $F_q = 2^{1/3}$ for the iso-heat-flux boundary conditions) are independent of the Grashof and Prandtl numbers. The data given in Table 10, in the range of Grashof and Prandtl numbers investigated, corroborate this generality of the deduced correction factors for the horizontal orientation of the heated plate.

5. Conclusion

It is shown that the theoretical average heat transfer coefficients for a semi-infinite horizontal plate needs to be corrected to account for the growth of boundary layers from both ends of a finite horizontal plate. For isothermal condition, it is mathematically deduced that $\overline{Nu}_{ht,corrected} = 2^{2/5}\overline{Nu}_{ht,theory}$, and, for constant-heat-flux condition it is mathematically deduced that $\overline{Nu}_{hq,corrected} = 2^{1/3}\overline{Nu}_{hq,theory}$. The mathematical deduction procedure reveals that these correction factors (dealing with the semi-infinite assumption in the similarity or integral theories) are independent of the Grashof and Prandtl numbers and this generality is demonstrated within the range of CFD investigation given in Table 10. It is noted that the deduced correction factors are large - the theoretical average Nusselt number changes by more than 30% for the isothermal case and by more than 25% for the iso-heat-flux case. The theoretical results for the average Nusselt number for a semi-infinite vertical plate, on the other hand, are reasonably close to the CFD results for a finite plate. This is so because, even in the case of a finite plate, a single boundary layer covers the entire length of a vertical plate (i.e. the physical situation is nearly the same as that assumed in the theories for semi-infinite plates).

An approximate theory (equation (17) or (19)) for the correction factor F_t is developed for the isothermal case for all near-horizontal inclination angles for which the lift-off point is located within the extent of the plate and hence two boundary layers form from the two edges of the plate. The expression for F_t produces correct limiting values, viz. $2^{2/5}$ for horizontal and 1 for vertical configurations, and brings previous theoretical results reasonably close to the CFD results, as shown in Fig. 6. Similarly, an approximate theory (equation (23) or (25)) for the correction factor F_q is developed for the iso-wall-heat-flux case for all near-horizontal inclination angles. The expression for F_q produces correct limiting values, viz. $2^{1/3}$ for horizontal and 1 for vertical configurations, and brings previous theoretical results reasonably close to the CFD results, as shown in Fig. 12.

The efficacy of the present methodology for near-horizontal inclination angles is demonstrated here at specific values of the Grashof and Prandtl numbers ($Gr_L = Gr_L^* = 10^6$, Pr = 0.7), but the same methodology may be applied at other values of Grashof and Prandtl numbers (requiring new CFD simulations at varying angles to determine the appropriate values of $\hat{L}_{LE}$ and $\hat{L}_{RE}$ in equations (17) and (23), and that of γ_m in equations (19) and (25) for the particular combination of Grashof and Prandtl numbers).

Great care is taken in the present work to obtain highly accurate CFD results that are well validated against experimental values. The present CFD simulations establish that (at $Gr_L = Gr_L^* = 10^6$, Pr = 0.7) there exists a minimum at near-horizontal positions both in the $\overline{Nu}_t$ versus γ and $\overline{Nu}_q$ versus γ curves. The process of deduction of the correction factors F_t and F_q helps in the comprehension of the physical reasons for the existence of a minimum in $\overline{Nu}$ for either isothermal or iso-heat-flux boundary condition. Table 4 for the isothermal case shows that $\overline{Nu}_t$ changes significantly as the inclination angle γ is increased from 15° to 60°, and the $\overline{Nu}_t$ versus $\bar{x}$ curve continues to increase (though slowly) in the range $60° < \gamma < 90°$. Table 7 shows that $\overline{Nu}_{q,CFD}$ is quite flat in the range $60° < \gamma < 90°$ and an additional feature is

noticed that there exists a small maximum at about $\gamma = 75°$.

The present study establishes the influence of the boundary condition - isothermal versus iso-wall-heat-flux - on the average Nusselt number for natural convection around a heated finite plate. At all inclinations, the isothermal case gives greater average Nusselt number ($\overline{Nu}_t > \overline{Nu}_q$, for $Gr_L = Gr_L^*$). The present study also establishes that, for the isothermal case, there is significant difference between the average Nusselt number (hence the overall heat transfer rate) for the horizontal and that for the vertical orientation of the plate. For example, at $Gr_L = 10^6$ and Pr = 0.7, $\overline{Nu}_{ht} = 12.4953$ and $\overline{Nu}_{vt} = 15.7941$, i.e. the overall heat transfer rate from a plate of finite length would increase by more than 25% if the orientation of the plate is changed from the horizontal to the vertical. At $Gr_L = 10^7$ and Pr = 0.7, it is found that $\overline{Nu}_{ht} = 19.7297$ and $\overline{Nu}_{vt} = 27.2746$, i.e. the increase in overall heat transfer rate is more than 35%. For the constant-heat-flux case, the change in average Nusselt number is modest. For example, at $Gr_L^* = 10^6$ and Pr = 0.7, $\overline{Nu}_{hq} = 9.7017$ and $\overline{Nu}_{vq} = 10.3027$, i.e. the overall heat transfer rate from a plate of finite length would increase only by 6% if the orientation of the plate is changed from the horizontal to the vertical. However, in the near-horizontal positions, the variation in the average Nusselt number with inclination angle is more prominent for the constant wall heat flux boundary condition as compared to the isothermal condition (Fig. 15).

Acknowledgement

The authors are grateful to Mr Debajyoti Das for his help with some of the computations. AG dedicates the mathematical deductions to his teachers.

Appendix

Unified Integral Theory Results

Algebraic expressions for local Nusselt number Nu_x are deduced in Refs. [2,16]. Appropriate integration of these expressions gives the corresponding average Nusselt numbers which are reported below. It is to be noted that the respective Prandtl number dependence in the following equations is mathematically deduced. ρ and χ are the orders of polynomials representing respectively the velocity profile and the temperature profile in the unified integral theory. The optimum values of ρ and χ for isothermal and constant-heat-flux conditions are determined in Refs. [2,16].

For isothermal vertical surface with $\lambda = 4$, $\chi = 2$, the Nusselt number ($\overline{Nu}_{vt}$) is given by:

$$\overline{Nu}_{vt} = 0.623\left(\frac{Gr_L \mathrm{Pr}^2}{\frac{5}{9} + \mathrm{Pr}}\right)^{1/4}. \tag{A1}$$

For isothermal horizontal surface with $\lambda = 4$, $\chi = 2$, the Nusselt number ($\overline{Nu}_{ht}$) is given by:

$$\overline{Nu}_{ht} = 0.722\left(\frac{Gr_L \mathrm{Pr}^2}{\frac{4}{9} + \mathrm{Pr}}\right)^{1/5}. \tag{A2}$$

Following the arguments advanced in Ref. [2] regarding local Nusselt number, it is suggested here that the average Nusselt number for arbitrary inclination for the isothermal plate is calculated from,

$$[\overline{Nu}_t(Gr_L,\ \mathrm{Pr},\ \gamma)]^n = [\overline{Nu}_{ht}(\cos\gamma)^{1/5}]^n + [\overline{Nu}_{vt}(\sin\gamma)^{1/4}]^n \tag{A3}$$

The advantage of equation (A3) is that it provides an explicit relation for $\overline{Nu}_t$, since $\overline{Nu}_{ht}$ and $\overline{Nu}_{vt}$ can be determined from equations (A2) and (A1). The Nusselt number given by equation (A3) correctly reduces to $\overline{Nu}_{ht}$ at $\gamma = 0°$ and to $\overline{Nu}_{vt}$ at $\gamma = 90°$. Ref [2] shows that $n = 5$ is a good choice and keeps the prediction of the correlation within ± 2% of the numerical results for the ranges of parameters investigated ($10^3 \le Gr_x \le 10^7$, $0.01 \le \mathrm{Pr} \le 100$, $0° \le \gamma \le 90°$).

For constant-heat-flux vertical surface with $\lambda = 3$, $\chi = 2$, the Nusselt number ($\overline{Nu}_{vq}$) is given by:

$$\overline{Nu}_{vq} = 0.77\left(\frac{Gr_L^* \mathrm{Pr}^2}{\frac{4}{5} + \mathrm{Pr}}\right)^{1/5}. \tag{A4}$$

For constant-heat-flux horizontal surface with $\lambda = 3$, $\chi = 2$, the Nusselt number ($\overline{Nu}_{hq}$) is given by:

$$\overline{Nu}_{hq} = 0.893\left(\frac{Gr_L^* \mathrm{Pr}^2}{\frac{4}{7} + \mathrm{Pr}}\right)^{1/6}. \tag{A5}$$

The average Nusselt number for arbitrary inclination for the iso-heat-flux case is calculated from,

$$[\overline{Nu}_q(Gr_L^*,\ \mathrm{Pr},\ \gamma)]^n = [\overline{Nu}_{hq}(\cos\gamma)^{1/6}]^n + [\overline{Nu}_{vq}(\sin\gamma)^{1/5}]^n \tag{A6}$$

The Nusselt number given by equation (A6) correctly reduces to $\overline{Nu}_{hq}$ at $\gamma = 0°$ and to $\overline{Nu}_{vq}$ at $\gamma = 90°$. Ref [2] shows that $n = 6$ is a good choice and keeps the prediction of the correlation within ± 1% of the numerical results for the ranges of parameters investigated ($10^3 \le Gr_x^* \le 10^7$, $0.01 \le \mathrm{Pr} \le 100$, $0° \le \gamma \le 90°$).

Similarity Theory Results

The similarity theory formula for average Nusselt number for an isothermal horizontal plate is derived in Ref. [15]:

$$\overline{Nu}_{ht} = -\frac{5}{3} {Gr_L}^{1/5} g'(0), \tag{A7}$$

where, $g'(0)$ is a function of the Prandtl number and is given in Table A1.

The similarity theory formula for average Nusselt number for an iso-heat-flux horizontal plate is derived in Ref. [15]:

$$\overline{Nu}_{hq} = \frac{6}{4}\ \frac{1}{18^{1/6}G(0)}\ (Gr_L^*)^{1/6}, \tag{A8}$$

where, $G(0)$ is a function of the Prandtl number and is given in Table A1.

Table A1
Values of $g'(0)$ and $G(0)$ in equations (A7) and (A8) respectively.

Pr	$-g'(0)$	$G(0)$
0.01	0.087650	3.65580
0.1	0.196149	1.88540
0.7	0.354304	1.18430
1	0.389570	1.09790
7	0.623621	0.75055
10	0.677046	0.70289
100	1.089644	0.46798
1000	1.747600	0.32039

The similarity theory formula for average Nusselt number for an isothermal vertical plate is derived in Ref. [4]:

$$\overline{Nu}_{vt} = \left(\frac{Gr_L}{4}\right)^{1/4} g(\mathrm{Pr}), \tag{A9}$$

where, $g(\mathrm{Pr})$ is a function of the Prandtl number and is given in Table A2.

Table A2
Values of $g(\mathrm{Pr})$ in equation (A9).

Pr	$g(\mathrm{Pr})$
0.01	0.1701510
0.1	0.3071254
0.7	0.6652302
1	0.7894452
10	1.5605743
100	2.2839181
1000	2.7466542

References

[1] P. Ganesan, G. Palani, Natural convection effects on impulsively started inclined plate with heat and mass transfer, Heat Mass Transf. 39 (4) (2003) 277–283.
[2] A. Guha, K. Pradhan, A unified integral theory of laminar natural convection over surfaces at arbitrary inclination from horizontal to vertical, Int. J. Therm. Sci. 111 (2016) 475–490.
[3] A. Guha, S. Sengupta, Effects of finiteness on the thermo-fluid-dynamics of natural convection above horizontal plates, Phys. Fluids 28 (6) (2016) 063603:1-29.
[4] A. Guha, S. Nayek, Thermo-fluid-dynamics of natural convection around a heated vertical plate with a critical assessment of the standard similarity theory, Phys. Fluids 29 (10) (2017) 103607:1-17.
[5] L.C. Burmeister, Convective Heat Transfer, second ed., John Wiley & Sons, New York, USA, 1993.
[6] W.M. Kays, M.E. Crawford, Convective Heat and Mass Transfer, third ed., McGraw-Hill, New York, USA, 1993.
[7] J.P. Holman, Heat Transfer, ninth ed., Tata McGraw-Hill, New Delhi, India, 2008.
[8] H. Schlichting, K. Gersten, Boundary-Layer Theory, eighth ed., Springer, New Delhi, India, 2004.
[9] O.A. Saunders, Natural convection in liquids, Proc. R. Soc. A 172 (1939) 55–71.
[10] R.J. Goldstein, E.R.G. Eckert, The steady and transient free convection boundary layer on a uniformly heated vertical plate, Int. J. Heat Mass Transf. 1 (2–3) (1959) 208–218.
[11] J. Gryzagoridis, Natural convection from a vertical flat plate in the low Grashof number range, Int. J. Heat Mass Transf. 14 (1) (1971) 162–165.
[12] M. Fishenden, O.A. Saunders, An Introduction to Heat Transfer, Oxford University Press, London, 1950.
[13] S. Ostrach, Report, An Analysis of Laminar Free Convection Flow and Heat Transfer about a Flat Plate Parallel to the Direction of the Governing Body Force vol. 1111, NACA, 1953.
[14] E.M. Sparrow, Tech. Note, Laminar free convection on a vertical plate with prescribed non uniform wall heat flux or prescribed non uniform wall temperature vol. 3508, NACA, 1955, pp. 1–34.
[15] S. Samanta, A. Guha, A similarity theory for natural convection from a horizontal plate for prescribed heat flux or wall temperature, Int. J. Heat Mass Transf. 55 (13–14) (2012) 3857–3868.
[16] A. Guha, S. Samanta, Closed-form analytical solutions for laminar natural convection on horizontal plates, ASME J. Heat Transf. 135 (10) (2013) 102501:1-9.
[17] Z. Rotem, L. Claassen, Natural convection above unconfined horizontal surfaces, J. Fluid Mech. 39 (1) (1969) 173–192.
[18] A. Guha, K. Pradhan, Natural convection of non-Newtonian power-law fluids on a horizontal plate, Int. J. Heat Mass Transf. 70 (2014) 930–938.
[19] K. Pradhan, S. Samanta, A. Guha, Natural convective boundary layer flow of nanofluids above an isothermal horizontal plate, ASME J. Heat Transf. 136 (10) (2014) 102501:1-9.
[20] K. Pradhan, A. Guha, Natural convection above a horizontal plate in a nanofluid-saturated porous medium with or without a magnetic field, J. Porous Media 18 (6) (2015) 613–628.
[21] K. Pradhan, A. Guha, CFD solutions for magnetohydrodynamic natural convection over horizontal and vertical surfaces, J. Mol. Liq. 236 (2017) 465–476.
[22] A. Guha, S. Sengupta, Non-linear interaction of buoyancy with von Kármán's swirling flow in mixed convection above a heated rotating disc, Int. J. Heat Mass Transf. 108 (Part A) (2017) 402–416.
[23] B.R. Rich, An investigation of heat transfer from an inclined flat plate in free convection, ASME J. Heat Transf. 75 (1953) 485–499.
[24] G.C. Vliet, Natural convection local heat transfer on constant-heat-flux inclined surfaces, ASME J. Heat Transf. 91 (4) (1969) 511–516.
[25] P. Sang-Urai, Investigation of Free Convection Heat Transfer from an Inclined Flat Plate, MS Thesis, University of Missouri-Rolla, 1969.
[26] T.S. Chen, H.C. Tien, B.F. Armaly, Natural convection on horizontal, inclined and vertical plates with variable surface temperature or heat flux, Int. J. Heat Mass Transf. 29 (10) (1986) 1465–1478.
[27] W.S. Yu, H.T. Lin, Free convection heat transfer from an isothermal plate with arbitrary inclination, Wärme-und Stoffübertragung 23 (4) (1988) 203–211.
[28] H.T. Lin, W.S. Yu, S.L. Yang, Free convection on an arbitrarily inclined plate with uniform surface heat flux, Wärme-und Stoffübertragung 24 (3) (1989) 183–190.
[29] S.C. Saha, J.C. Patterson, C. Lei, Natural convection boundary-layer adjacent to an inclined flat plate subject to sudden and ramp heating, Int. J. Therm. Sci. 49 (9) (2010) 1600–1612.
[30] A. Guha, A. Jain, K. Pradhan, Computation and physical explanation of the thermo-fluid-dynamics of natural convection around heat inclined plates with inclination varying from horizontal to vertical, Int. J. Heat Mass Transf. 135 (2019) 1130–1151.

[31] B. Gebhart, Effect of viscous dissipation in natural convection, J. Fluid Mech. 14 (2) (1962) 225–232.
[32] Ansys Inc., ANSYS FLUENT 14.5 User's Guide, (2009).
[33] A. Guha, S. Samanta, Effect of thermophoresis on the motion of aerosol particles in natural convective flow on horizontal plates, Int. J. Heat Mass Transf. 68 (2014) 42–50.
[34] A. Guha, S. Samanta, Effect of thermophoresis and its mathematical models on the transport and deposition of aerosol particles in natural convective flow on vertical and horizontal plates, J. Aerosol Sci. 77 (2014) 85–101.
[35] J.R. Lloyd, E.M. Sparrow, E.R.G. Eckert, Laminar, transition and turbulent natural convection adjacent to inclined and vertical surfaces, Int. J. Heat Mass Transf. 15 (3) (1972) 457–473.
[36] P.E. Dimotakis, The mixing transition in turbulent flows, J. Fluid Mech. 409 (2000) 69–98.
[37] Y. Mei, A. Guha, Implicit numerical simulation of transonic flow through turbine cascades on unstructured grids, Proc. Inst. Mech. Eng. Part A 219 (1) (2005) 35–47.
[38] A. Guha, J.B. Young, Time-marching Prediction of Unsteady Condensation Phenomena Due to Supercritical Heat Addition, In Turbomachinery: Latest Developments in a Changing Scene, Institution of Mechanical Engineers, London, UK, 1991, pp. 167–177.
[39] A. Guha, Thermal choking due to nonequilibrium condensation, ASME J. Fluids Eng. 116 (3) (1994) 599–604.
[40] J. Gryzagoridis, Natural convection from a vertical flat plate in the low Grashof number range, Int. J. Heat Mass Transf. 14 (1) (1971) 162–165.
[41] E.M. Sparrow, C.K. Carlson, Local and average natural convection Nusselt numbers for a uniformly heated, shrouded or unshrouded horizontal plate, Int. J. Heat Mass Transf. 29 (3) (1986) 369–379.
[42] E.M. Sparrow, J.L. Gregg, Laminar free convection from a vertical plate with uniform surface heat flux, ASME J. Heat Transf. 78 (1956) 435–440.